communications biology

A Nature Portfolio journal

Article

https://doi.org/10.1038/s42003-025-08765-7

Immunoproteasome remodeling in senescing human macrophages reveals the loss of PA28αβ capping as a hallmark of immunosenescence

Francesca Monittola, Sofia Masini, Mariele Montanari, Maria Gemma Nasoni, Marzia Bianchi, Rita De Matteis, Anastasia Ricci, Daniela Ligi, Francesca Luchetti, Barbara Canonico, Mauro Magnani, Michele Menotta, Alessandra Fraternale & Rita Crinelli ✉

Aging negatively impacts proteasome activity and/or content, and this impairment contributes to disrupted protein homeostasis and cellular dysfunction. However, little is known about proteasome complex dynamics during aging, particularly in the context of immunosenescence. Indeed, only limited data are available on the immunoproteasome, a specialized variant expressed in immune cells. We establish an in vitro model of monocyte-derived human macrophages that develop a senescence-like phenotype upon long-term culture. Our data demonstrate that immunoproteasome complexes undergo deep structural and functional alterations, with the downregulation of immunosubunit expression at the mRNA and protein level, uncapping of the 20S catalytic particle by the PA28αβ regulator, and loss of activity. Immunosubunits are partly replaced by their constitutive counterparts with a shift toward the building of 19S-capped 20S complexes to maintain proteostasis. Similar proteasome dynamics are found in the lymph nodes of aged C57BL/6 and BTBR mice, the latter of which have a naturally activated immune system. Overall, these findings propose long-term cultures of human monocyte-derived macrophages as a model to study macrophage senescence. They also provide a molecular rationale for immunoproteasome dysfunction with remodeling of the proteasome, indicating that the loss of the PA28αβ regulator is a critical event and a hallmark of immunosenescence.

Immunosenescence is a process that leads to a general decline in immune function with increasing age. Macrophages are cells of the innate immune system that play different roles in several physiological processes, such as the immune response, tissue homeostasis and inflammation[1]. Macrophages are long-lived cells originating from embryonic precursors as well as from monocytes (MOs), including circulating blood MOs. Although macrophages are mature differentiated cells, it has been recently demonstrated that they maintain self-renewal properties[2]. However, once activated, macrophages engage in a rapid proinflammatory response and lose their ability to proliferate; this process is thought to limit pathogen spread and/or proinflammatory cytokine overproduction[3,4]. Among the cell cycle regulators which are differentially expressed after activation, $p21^{Waf1/Cip1}$ is upregulated to prevent apoptotic death[5,6]. Therefore, these cells may survive after the resolution of inflammation and persist within tissues where they maintain an inflammatory signature for a certain period[7,8]. Whether this condition can lead to the onset of senescence is a matter of debate[9].

Senescent cells are characterized by several features that are not exclusive or essential, as the senescence process is stress- and cell type dependent. Despite phenotype heterogeneity, a general set of senescence markers has been identified, and they are routinely used to assess the senescent state. Typical markers include the activation of the cyclin-dependent kinase (CDK) inhibitors $p21^{Waf1/Cip1}$ and $p16^{INK4a}$; lysosomal expansion with increased senescence-associated β-galactosidase (SA-β-gal) activity at pH 6.0; the build-up of lipofuscin granules containing oxidized

Department of Biomolecular Sciences, University of Urbino Carlo Bo, Urbino (PU), 61029, Italy.
✉e-mail: rita.crinelli@uniurb.it

proteins, lipids and metals; the secretion of proinflammatory factors (SASPs); and the acquisition of a flattened and enlarged cell shape[10].

Many of these features have been described in lipopolysaccharide-stimulated macrophages and in irradiated bone marrow-derived monocytes/macrophages (BMMs) as well as ex vivo in cultured brain microglia and in vivo in tissues of aged mice and in disease models such as gliosis or periodontitis[11–15].

The effects of immunosenescence on macrophage functions are well known[16], but fundamental questions remain unanswered, including how protein homeostasis is maintained and proteostatic pathways are regulated. Recent studies have shown that proteasome dysfunction leads to a senescent-like phenotype[17]. However, the characterization of proteasome dynamics and the role of this proteolytic complex in senescent cells remain elusive from both molecular and functional perspectives, especially in immune cells, which express a specialized variant of the standard proteasome called the immunoproteasome[18].

The proteasome is a multicatalytic complex that degrades unfolded/damaged proteins as well as regulatory proteins. The constitutive proteasome consists of a catalytic core made of α and β rings where the β1, β2 and β5 subunits are catalytically active. Three different proteolytic activities are associated with the 20S particle: caspase (or peptidyl glutamyl hydrolytic), trypsin and chymotrypsin-like activities[18]. The three catalytic β-subunits are replaced by their counterparts β1i (LMP2), β2i (MECL-1) and β5i (LMP7) to form the immunoproteasome (i20S). The immunoproteasome shapes the repertoire of antigenic peptides and regulates cytokine production under proinflammatory conditions, but it is also thought to be involved in maintaining protein homeostasis[18,19].

The activity of the 20S core can be regulated by capping with regulatory particles such as the 19S complex, which catalyzes proteasome-driven ATP and ubiquitin (Ub)-mediated proteolysis, and the PA28αβ (11S) regulator, which is ATP- and Ub-independent as well as interferon-γ (IFN-γ)-inducible. In both cases, association with regulatory particles increases 20S activity and likely the nature of the released peptides[20,21]. The 19S complex consists of two parts: a base composed of six AAA + -ATPase subunits (Rpt1-Rpt6) directly contacting the α ring of the CP and four non-ATPase subunits (Rpn1, Rpn2, Rpn10 and Rpn13) and a lid composed of nine non-ATPase subunits (Rpn3, Rpn5-Rpn9, Rpn11, Rpn12, and Sem1/Rpn15). Rpn 10 seems to bind mainly to the lid. Conversely, PA28αβ is a heteroheptameric complex of two highly homologous subunits, i.e., PA28α and PA28β, with a stoichiometry of $\alpha_4\beta_3$[22,23].

Here, we provide evidence that in an in vitro model of human senescent macrophages, immunoproteasome and PA28αβ subunit levels irreversibly decreased but were in part replaced with their constitutive counterparts and the build-up of 19S-capped complexes. Changes in composition may be part of an adaptive response that allows senescent cells to cope with proteostasis collapse and survive. The same features could be observed in vivo in the lymph nodes of two murine models of aging, suggesting that PA28αβ downregulation and the consequent proteasome remodeling are hallmarks of immunosenescence.

Results

Establishment of an in vitro model of senescent human macrophages

Understanding the molecular mechanisms that drive macrophage senescence is limited by the availability of in vitro models that mimic in vivo processes. Studies are mostly based on immortalized monocyte/macrophage lines stimulated with various stressors, raising concerns as to whether and to what extent they can recapitulate natural senescence[24–26]. A recent comparative analysis proposed lipopolysaccharide-stimulated murine peritoneal macrophages as the model with the greatest similarity to macrophages isolated from aged mice[27]. Few studies have investigated age-related changes in human macrophages, with even fewer involving primary cells[28]. Human macrophages are usually obtained from the in vitro differentiation of blood monocytes that can be isolated from waste products of blood components in sufficient amounts for protocols requiring high numbers of cells. Monocyte-derived macrophages are indeed considered a source of cells for studying macrophage biology[29]. On the basis of these considerations, we developed an in vitro system of blood-derived monocytes differentiated into macrophages (MDMs) that were subsequently induced to acquire a senescent-like phenotype in long-term culture.

To obtain terminally differentiated macrophages, monocytes were separated from lymphocytes by plastic adhesion and cultured in the absence of exogenously added proliferation/growth factors. Indeed, cell attachment has been demonstrated to be sufficient to trigger monocyte-to-macrophage differentiation, and stimuli other than macrophage colony-stimulating factors can promote the differentiation of monocytes into macrophages[30–32].

After 7 days of culture, monocytes differentiated into macrophages (Mφs), as evidenced by changes in cell morphology with the acquisition of an enlarged and flattened shape, an increased cytoplasm/nucleus ratio, pseudopods, and a vacuolar system (Fig. 1a). Another feature of macrophage differentiation was enhanced granularity, as shown by an increase in side scatter (SSC) on flow cytometry (Supplementary Fig. 1a)[33]. Moreover, labeling with specific antibodies revealed the significant upregulation of the macrophage markers CD68, CD64, CD14, CD11b, CD11c, CD206, CD80 and TLR4 compared with those on day 0 (i.e., monocytes), demonstrating that the cells had acquired a macrophage-like phenotype[34]. Moreover, the phagocytosis of pHrodo green zymosan nanoparticles, which fluoresce only under acidic conditions, indicated increased phagolysosome formation and maturation, a key function of mature macrophages (Supplementary Fig. 1b)[35].

Upon prolonged culture, cycling and postmitotic cells, such as primary neurons and peritoneal macrophages, develop a senescent-like phenotype[36–38]. Moreover, chronic but not acute senescence is associated with a state of deep senescence, which involves adaptation[39]. Thus, to study the mechanisms of adaptation, we opted to establish extended cultures in which the cells gradually acquired a senescent-like state. To this end, differentiated Mφs (7 days) were maintained in culture for 3 more weeks, and the expression of multiple well-established senescence markers was evaluated at 7, 14 and 28 days post cell seeding in one- (14 days) and three-week-old (28 days) macrophages.

In the time window 7–28 days, cell viability did not change as demonstrated by similar intracellular lactate dehydrogenase activity (LDH). Cell death by necrosis, as determined by LDH release in the culture medium, was maximum at 7 days, then decreased and remained stable until 28 days (Supplementary Fig. 1a). Overall, these data indicate that, under our experimental conditions, macrophage differentiation and activation were inherently stressful, as also reported by others[32], whereas prolonged culture did not negatively affect cell survival. During this time, macrophages maintained strong CD11b, CD11c, TLR4, CD206 and CD80 staining, supporting their mature macrophage phenotype. Moreover, the percentage of cells expressing the M1 and M2 macrophage markers CD206, TLR4 and CD80 did not change over time, suggesting that Mφs polarized toward a mixed M1/M2 phenotype, which was maintained until day 28 (Supplementary Fig. 1b).

Stable cell cycle arrest in the form of $p21^{Waf1/Cip1}$ or $p16^{INK4a}$ expression is the primary marker used to assess cell senescence. However, the activation of $p21^{Waf1/Cip1}$ is essential for the differentiation of monocytes into macrophages[5,40]. Therefore, the accumulation of $p21^{Waf1/Cip1}$ is not sufficient to establish a condition of senescence in these cells. In addition, while the expression of $p21^{Waf1/Cip1}$ is necessary for induction, the coexpression of $p16^{INK4a}$ is required to maintain a senescent state[41]. Accordingly, on day 7, the macrophages expressed $p21^{Waf1/Cip1}$ but not $p16^{INK4a}$ (Fig. 1b, c). In contrast, on day 14, $p21^{Waf1/Cip1}$ protein levels increased compared with those in 7-day Mφs, and $p16^{INK4a}$ de novo synthesis was detected via western immunoblot analysis (Fig. 1b, c). Confocal fluorescence microscopy revealed that, in most of the Mφs, the two cell cycle inhibitors were expressed within the same cell and had a prevalent cytoplasmic localization (Fig. 1d). Cytoplasmic $p21^{Waf1/Cip1}$ is thought to have antiapoptotic rather than cell cycle inhibitor functions[6,42]. The levels and localization of $p16^{INK4a}$ are controlled by the autophagy pathway, thus inhibition of autophagy leads to

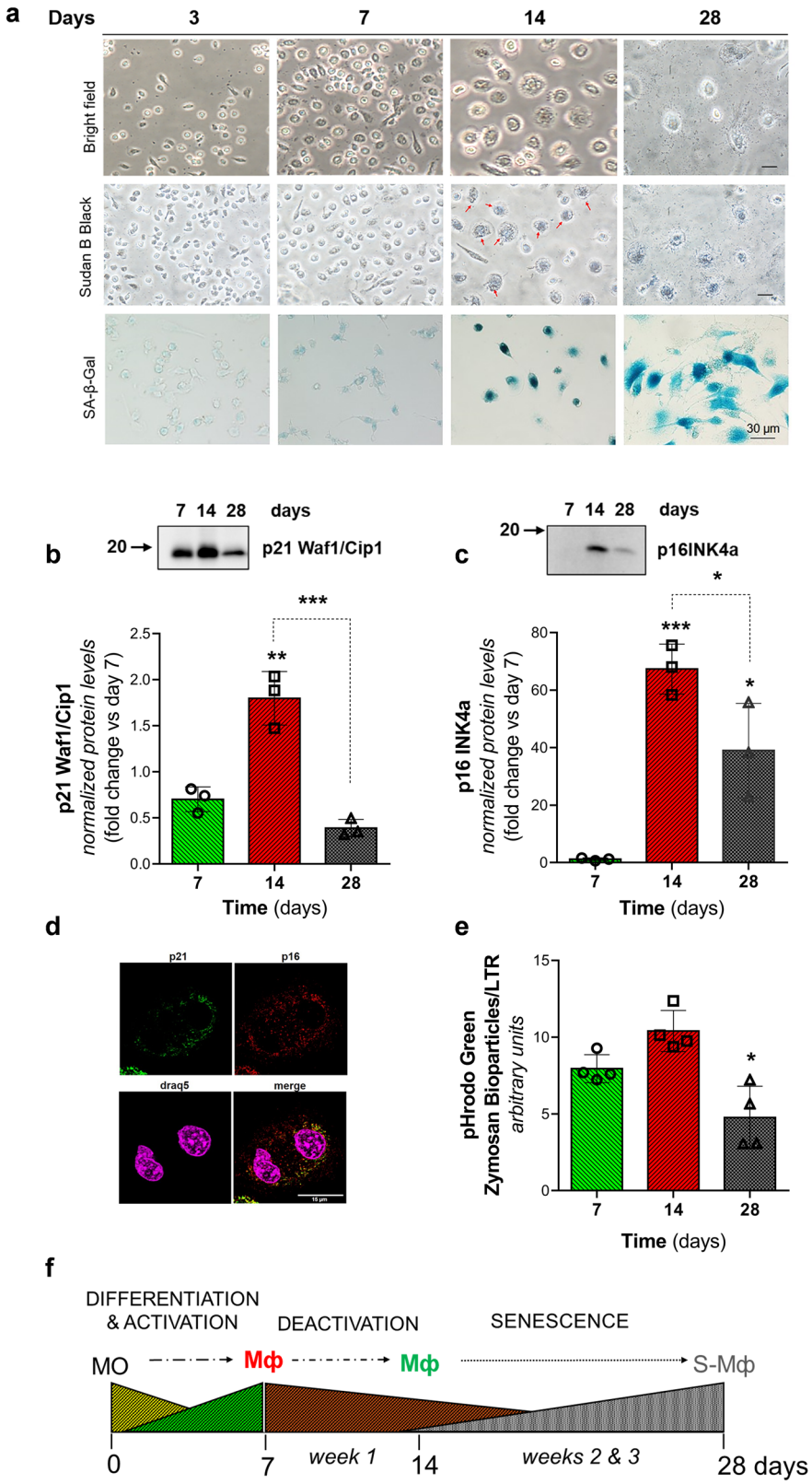

Fig. 1 | Analysis of senescence markers in long-term cultures of human monocyte-derived macrophages and schematic representation of the experimental model. a Optical microscope images of cells left unstained (Bright field) and stained with Sudan B black or for (SA)β-gal activity. Red arrows indicate lipofuscin-positive cells. Scale bars 30 μm. Cells were analyzed after 3, 7, 14 and 28 days of culture. **b** Five micrograms of total protein (for the detection of p21Waf1/Cip1) and (**c**) 10 μg of total protein (for the detection of p16INK4a) were separated via SDS-PAGE on a 14% (w/v) acrylamide gel and subjected to western immunoblotting with specific antibodies. The total protein content in each lane was detected using No Stain reagent as a loading control. Immunoreactive bands and total protein signals were imaged with a ChemiDoc system and quantified with Image Lab software. The values were normalized to the total protein content and are reported in the graph as the fold change vs. day 7. Data are the mean ± S.D. $^{*}p < 0.05$; $^{**}p < 0.01$; $^{***}p < 0.005$. **d** Coexpression of the p21Waf1/Cip1 and p16INK4a proteins by immunofluorescence confocal microscopy at 14 days. Nuclei were stained with DRAQ5 reagent, and images were captured using a confocal Leica microscope (63× oil objective). Scale bar 15 μm (**e**) Phagocytosis/lysosomal activity was assessed by flow cytometry using a pHrodo Green Zymosan BioParticles Conjugate assay kit. MFI signals were normalized to the lysosome content, as determined by LysoTracker Red (LTR) staining. Data are the mean ± S.D. ($^{*}p < 0.05$). **f** After PMBC isolation, monocytes (M0) were separated from lymphocytes by plastic adhesion and cultured for up to 28 days; after 7 days of culture, adherent MOs (yellow) differentiated into activated macrophages (Mϕs, red); if kept in culture for up to 3 weeks, Mϕs were deactivated over time (Mϕ, green), and a senescence-like phenotype developed (S-Mϕ, gray). On the basis of senescent marker expression, day 14 coincided with the onset of senescence, and day 28 coincided with the senescent state.

the accumulation of $p16^{INK4a}$ in the cytosol, which is believed to contribute to the induction of senescence[43]. Both cell cycle inhibitors remained highly expressed on day 28, with significantly higher expression than that observed on day 7 in the case of $p16^{INK4a}$ (Fig. 1b, c). Cell cycle analysis by flow cytometry revealed that more than 90% of the cells were in the G0/G1 phase with less than 2% of apoptotic cells (Supplementary Fig. 2a). Irreversible cell cycle arrest was also demonstrated by a significant decrease in proliferating cell nuclear antigen (PCNA) levels on day 28, as determined by proteomic analysis (Supplementary Fig. 2b). Consistently, the cell proliferation antigen Ki-67 was undetectable on day 7 in 3 out of the 4 cell cultures obtained from different donors and was completely absent in all the samples at the other time points (Supplementary Fig. 2c). PCNA and Ki-67 expression was

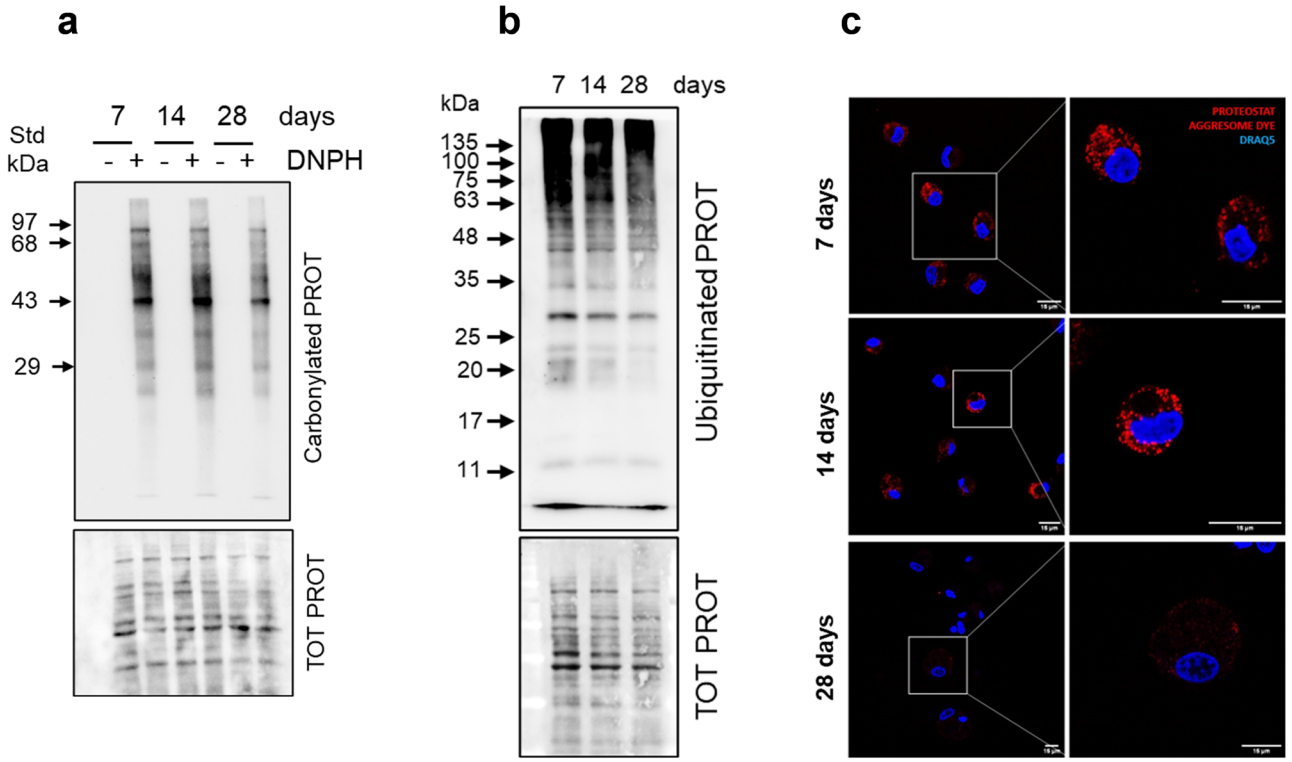

Fig. 2 | Protein carbonylation, ubiquitination and aggresome formation. **a** Protein carbonylation, as detected with an OxyBlot kit. Five micrograms of protein derivatized with DNPH and nonderivatized, as a negative control, were separated by SDS-PAGE on a 12% (w/v) acrylamide gel and subjected to Western immunoblotting with an anti-DNPH antibody. Total protein was visualized as a loading control. **b** Ubiquitin-conjugated proteins were detected by western immunoblotting with an antibody directed against ubiquitin. Five micrograms of total protein was separated via SDS-PAGE on a 13% (w/v) acrylamide gel. Total protein was used as a control. **c** Aggresomes were detected with a ProteoStat® Aggresome Detection Kit in accordance with the manufacturer's instructions. DRAQ5 was used to visualize the nuclei (blue). Images were acquired with a confocal Leica microscope (×63 oil objective) using a standard rhodamine filter set. Scale bars 15 µm.

confirmed by western immunoblot analysis and confocal microscopy, respectively (Fig. 2b, c).

Starting from day 14, Mφs exhibited morphological changes typical of senescent cells, with the acquisition of a larger and/or flattened morphology, accumulation of lipofuscin granules, and presence of senescence-associated-β-galactosidase (SA-β-Gal) activity (Fig. 1a), which became more evident on day 28. Moreover, these cells presented diminished phagolysosome activity, as demonstrated by decreased zymosan nanoparticle uptake into acidified phagolysosomes, which was normalized to the total lysosome content (Fig. 1e). On the basis of these results and in accordance with the idea that senescence is a dynamic multistep process[39], we distinguished two phases: a senescence initiation stage (after 14 days in culture), which is characterized mainly by permanent cell cycle exit, and a fully senescent stage (after 28 days in culture), which features morphological changes and alterations in lysosomal/phagocytic functions.

An analysis of a panel of secreted cytokines in culture medium revealed that the macrophages displayed a secretory phenotype on day 7 (Supplementary Fig. 3a). Recently, -IFN-γ was shown to drive the differentiation of blood-derived human monocytes into macrophages, leading to bona fide macrophages with inflammatory characteristics[32]. Therefore, these cytokines may provide stimuli that promote the differentiation of monocytes into macrophages in the absence of growth factors, allowing the establishment of a model that may better mimic a naturally occurring inflammation-induced senescence phenotype. Indeed, cytokine levels decreased over time, revealing early macrophage activation and subsequent deactivation upon extended culture. Although this condition does not allow us to clearly appreciate the appearance of a senescence-associated secretory phenotype, some cytokines were still detectable until day 28 under nonstimulated conditions (Supplementary Fig. 3a). Whether the cells are still in the deactivation phase or retain a low level of chronic inflammation, characteristic of the senescent state, it is difficult to determine. The most abundant cytokines were TNF-α, IL-8 and IL-10. Among the cytokines assessed, IL-18, IL-8 and IL-10 showed the slowest rates of decay, particularly IL-18, which has been shown to promote fibroblast replicative senescence[44] (Supplementary Fig. 3b). Similarly, it has been recently demonstrated that IL-10 is the primary elevated cytokine associated with the secretory phenotype of senescent-like macrophages in endplate sclerosis[45].

Overall, our model involved (1) an activation/differentiation step from day 0 to day 7 characterized by the increased expression of macrophage markers and cytokine secretion; (2) a deactivation phase from day 7 to day 28 with a decrease in cytokine secretion; and (3) a senescent phase, beginning on day 14 with the expression of cell cycle inhibitors and SA-βGal activity and becoming evident on day 28 with the disappearance/decrease in cell proliferation factors, morphological changes, strong SA-βGal staining, lipofuscin accumulation, impaired phagolysosome activity and low levels of cytokine secretion (Schematic representation in Fig. 1f). The proteomic characterization of the senescent model can be found in the supplementary material (Supplementary Figs. 4 and 5 and Supplementary Data 1–3).

Macrophage activation is accompanied by proteostasis disturbances that are resolved during the senescence phase

Since cellular proteostasis decreases during human senescence and prolonged disturbance of this process induces senescence, we initially investigated the expression of markers of proteome damage[46,47]. Figure 2a shows representative images of carbonylated proteins as determined by a commercially available OxyBlot™ protein oxidation detection kit.

Protein carbonylation was detectable at 7 days; however, the oxidized protein levels decreased with time. The ubiquitin proteasome system maintains protein homeostasis by removing misfolded and/or damaged proteins to prevent their accumulation within cells. Western immunoblot

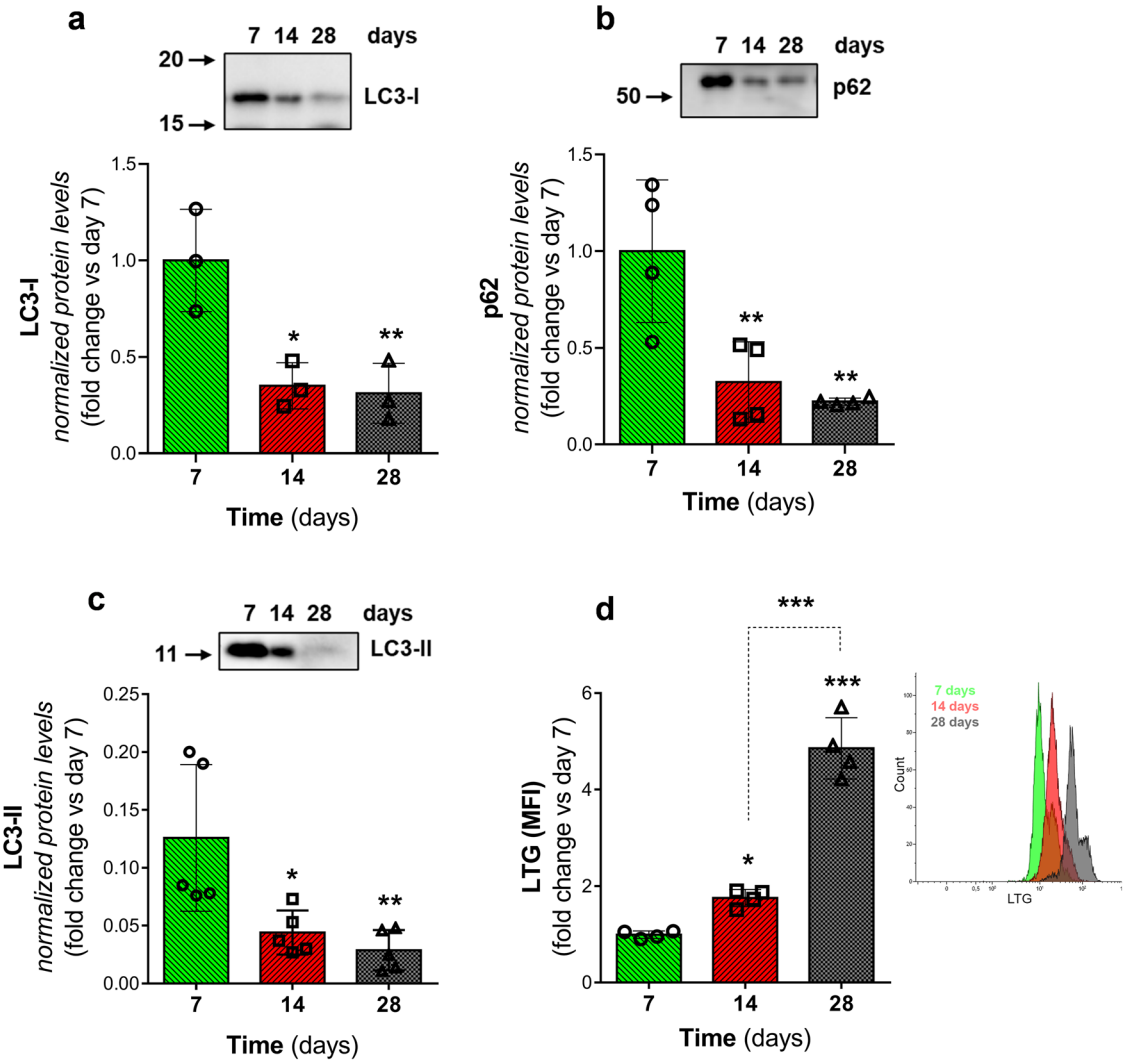

Fig. 3 | Analysis of the autophagy/lysosome system. Representative western immunoblot analysis of LC3 protein (**a**, **c**) and SQSTM-1/p62 receptor (**b**) levels. LC3-I precursor cellular content was determined under basal conditions (**a**), while its lipidated activated form, LC3-II, was investigated after chloroquine treatment (**c**) to evaluate autophagosome formation. Five micrograms of total protein (for the detection of LC3) were separated by SDS-PAGE on a 14% (w/v) acrylamide gel. For p62, 10 μg of total protein was separated on a 10% (w/v) acrylamide gel. Densitometric values of immunoreactive bands were normalized to total protein and are reported in the graphs as the fold change vs day 7. **d** LysoTracker Green (LTG) dye was used to mark and trace the lysosomes. The fluorescent signal was acquired and quantified by flow cytometry. Data are the mean ± S.D. $*p < 0.05$; $**p < 0.01$; $***p < 0.005$. A representative histogram overlay is shown in the right panel. The gating strategy is shown in Supplementary Fig. 1a.

analysis of ubiquitin and Ub-conjugated proteins revealed that the amount of oxidized proteins coincided with decreased pools of polyubiquitinated proteins (Fig. 2b). In parallel, PROTEOSTAT dye staining, which stains protein aggregates, revealed a high percentage of positive cells with numerous bright puncta on day 7 (Fig. 2c). The dye detects ALISs (aggresome-like induced structures), i.e., inclusion bodies of aggregated, misfolded proteins that are formed when the ubiquitin–proteasome protein-degradation machinery is overwhelmed and that are usually cleared through autophagic degradation[48]. The intensity of the signal and the number of puncta decreased with time. On day 28, the cells displayed lower and more diffuse staining than did the activated macrophages. Taken together, these findings demonstrate that macrophage activation on day 7 was accompanied by proteostasis stress, in agreement with the knowledge that cytokine stimulation causes proteostasis disturbances and probably overloads proteolytic systems[49]. This phase was followed by a slow recovery phase that began during deactivation toward the restoration of proteostasis on day 28, suggesting that cells can reprogram their protein metabolism to limit proteome damage and survive.

Macrophage senescence is accompanied by a decline in the autophagy/lysosome system

To investigate the molecular mechanism of cell adaptation, the functionality of the proteolytic pathways involved in protein homeostasis maintenance was analyzed, starting from the autophagy and lysosome systems, which usually decline in cellular and immune senescence[50]. Western immunoblot analysis of the autophagy markers microtubule-associated protein 1A/1B light chain 3B (LC3) and p62 revealed significant decreases in the LC3-I precursor and p62 cellular contents at 14 days compared with those observed in 7-day differentiated macrophages (Fig. 3a, b).

After treatment with chloroquine, which inhibits the fusion process between autophagosomes and lysosomes, the amount of accumulated LC3-II decreased, supporting the conclusion that the ability of the cells to assemble new autophagosomes was reduced (Fig. 3c). Moreover, lysosome accumulation was detected on day 28, indicating general impairment of the autophagosome/lysosome system (Fig. 3d). This observation could also explain the appearance of lipofuscin starting on day 14 (Fig. 1a). GO analysis of the proteomic data confirmed the regulation of macroautophagy

(Supplementary Fig. 5, in purple) starting from day 14, with 8 differentially expressed proteins, including p62 (SQSTM1) and LC3 (MAP1LC3B), as determined by western immunoblot analysis. On day 28, at least 20 factors involved in autophagosome formation were found to be differentially expressed, providing a molecular framework for observing the general impairment of the ability of the cells to form autophagosomes (Supplementary Fig. 6).

The decline in the autophagic/lysosomal system suggests that other proteolytic machinery may be involved in proteostasis maintenance.

Proteasome machinery is remodeled during macrophage senescence

Immunoproteasome subunits are the most abundant proteasome components expressed in immune cells[51]. However, whether the immunoproteasome contributes to maintaining protein homeostasis is a matter of debate[18]. In addition, while proteasome activity and/or levels decline in senescent cells, little is known about the fate of the immunoproteasome, especially in immune cells. Therefore, we next focused our analyses on the expression, proteolytic complex assembly and activity of the immunoproteasome in senescent macrophages.

Compared with those in mature macrophages, the levels of the immunoproteasome subunits β5i (*PSMB8*) and β1i (*PSMB9*) were lower at both the mRNA and protein levels (Supplementary Fig. 7 and Fig. 4).

The decrease in mRNA expression (14 days) preceded that in protein expression on day 28. The loss of β1i and β5i was apparently counterbalanced by the increased expression of the constitutive counterparts β1 and β5, suggesting the occurrence of a compensatory mechanism. On the other hand, the overall proteasome content did not apparently change, as demonstrated by an equal amount of α subunits detected by western immunoblotting with a pan α antibody. We also analyzed the expression of the PA28β and Rpt4 proteins to trace the PA28αβ and 19S regulatory complexes, respectively, and found that PA28β expression was downregulated only on day 28 (Fig. 4).

In addition to the downregulation of the expression of immune subunits and PA28β and the upregulation of the expression of the constitutive β5 subunit, proteomic analysis highlighted changes in the expression levels of several other factors involved in proteasome assembly and function (Fig. 5). Notably, the downregulation of the expression of PA28α, which together with PA28β form the PA28αβ (11S) particle, suggests the broad involvement of this proteasome regulator in macrophage senescence. The downregulation of the expression of α subunits and a few constitutive β subunits, starting with α6/β6 on day 14 and involving almost all the other α subunits on day 28, suggests that the expression of α rather than β-type subunits may limit the assembly of the constitutive 20S proteasome. Another interesting observation is a transient rearrangement of the 19S lid occurring at the onset of the senescent-like phenotype (i.e. 14 days), with the upregulation of Rpn3 expression, downregulation of Rpn10 expression, and loss of some 19S base subunits on day 28, indicating that the plasticity of this complex may play an important role in cell adaptation and proteostasis maintenance.

Since the biogenesis of the proteasome is regulated at the transcription, translation and molecular assembly levels, subunit incorporation into active proteasome complexes was studied by native PAGE analysis followed by western immunoblotting. Indeed, the abundance of various proteasome subunits within cells may not necessarily reflect their assembly within active proteasomes[52]. Staining with the pan α antibody revealed two main proteasome complexes in mature macrophages (day 7) (Fig. 6a).

The most abundant and faster migrating particle was identified as the 20S core particle (CP) capped with the PA28αβ regulator, which was immunoreactive to an anti-PA28β antibody. Within the resolution limit of our gels, we never detected two distinct bands in this region; therefore, we cannot exclude the presence of uncapped 20S that comigrates with the 20S/PA28αβ proteasome. The higher molecular weight complex corresponded to the 26S proteasome, i.e., the 20S core particles capped with the 19S regulator, as demonstrated by staining with an antibody against the 19S ATPase subunit Rpt4. Additional faint bands migrating above the 26S complex were revealed by antibodies against panα subunits and were further identified as the 30S complex (19S doubly capped 20S), stained by the anti-Rpt4 antibody, and the hybrid immunoproteasome 19S/20S/PA28αβ immunoreactive to both anti-Rpt4 and anti-PA28β antibodies. An analysis of the complexes at the subsequent time points confirmed the loss of immunoproteasome subunits and the increased incorporation of their constitutive counterparts, with the gradual disappearance of PA28αβ-capped core particles in favor of the formation of 19S-capped complexes, including the 30S proteasome. The normalization of PA28β, β5i and β5 immunoreactive signals to the panα signal of the 20S/PA28αβ particle to compensate for decreased proteasome content confirmed the loss of PA28αβ capping and interchange between subunits (Supplementary Fig. 8a). Consistently, the β5i activity assayed in cell-free extracts with the fluorogenic peptide ANW-AMC decreased, but the overall chymotrypsin-like activity of the proteasome also decreased over time, as determined using the sLLVY-AMC substrate (Fig. 6b). Since peptide hydrolysis requires the ability of regulatory particles (RPs) to form complexes with the CP and open the gate for substrate entry into the catalytic sites, gel peptidase assays were performed to provide further evidence of regulatory particle assembly with the 20S catalytic core particle. Gel activity assays clearly demonstrated that most chymotrypsin-like activity was catalyzed by the PA28αβ-capped immunoproteasome in mature macrophages, with a modest contribution from the 26S proteasome. In contrast, both the residual PA28αβ-capped 20S complexes and the 19S-capped CP, including the de novo assembled 26S and 30S proteasomes, contributed to proteasome activity in senescent cells (Fig. 6b). Similar results were obtained when fluorogenic substrates specific for β5i, β1i, and trypsin-like activities were used, which also allowed the incorporation of immunosubunits into 30S complexes to be observed (Supplementary Fig. 8b). Taken together, this evidence demonstrates that during macrophage senescence, not only does the content and activity of the immunoproteasome complexes decrease but this decline is also accompanied by deep proteasome complex remodeling. In particular, the replacement of immunosubunits with constitutive ones and the loss of PA28αβ capping of the 20S particle, with a shift toward the assembly of 19S-capped complexes, could be part of a possible compensatory mechanism to maintain proteostasis.

Interferon-γ stimulation does not restore immunoproteasome subunit or PA28β expression in senescent macrophages

PA28αβ subunits are constitutively expressed in immune cells but can also be induced by IFN-γ, whose levels drastically decreased between 7 and 14 days of culture (Supplementary Fig. 3b). Therefore, we next assessed whether the observed changes in proteasome content and composition were due to cell deactivation rather than senescence. Macrophages were stimulated with IFN-γ for 24 h, and the levels of β5i and PA28β were analyzed by western immunoblotting. As shown in Fig. 7a, IFN-γ did not restore the intracellular content of either protein in senescent cells (28 days).

Quantification of the immunoreactive signal in extracts obtained from cells derived from 3 different donors revealed that the ratio of IFN-γ-stimulated to basal levels (unstimulated cells) was 1.1 ± 0.2 S.D. for β5i and 1.06 ± 0.17 S.D. for PA28β. Native PAGE analysis of proteasome complexes confirmed the inability of senescent cells to respond properly to IFN-γ stimulation (Fig. 7b). β5i incorporation into the 20S proteasome and activity (ANW-AMC hydrolysis) were moderately increased in mature macrophages (7 days) after IFN-γ treatment, probably because the cells were already stimulated. The gel activity results demonstrated that β5i activity was mostly catalyzed by the 20S/PA28αβ complex. In contrast, in stimulated senescent macrophages (28 days), the β5i immunosubunit was partially reincorporated into proteasome complexes; however, these particles were mostly inactive because of the inability to restore PA28αβ levels and to reconstitute capped 20S holoenzymes. Likewise, the assembly of the constitutive β5 subunit into the 20S core and its incorporation into 19S-capped complexes were not affected by IFN-γ, clearly demonstrating that the

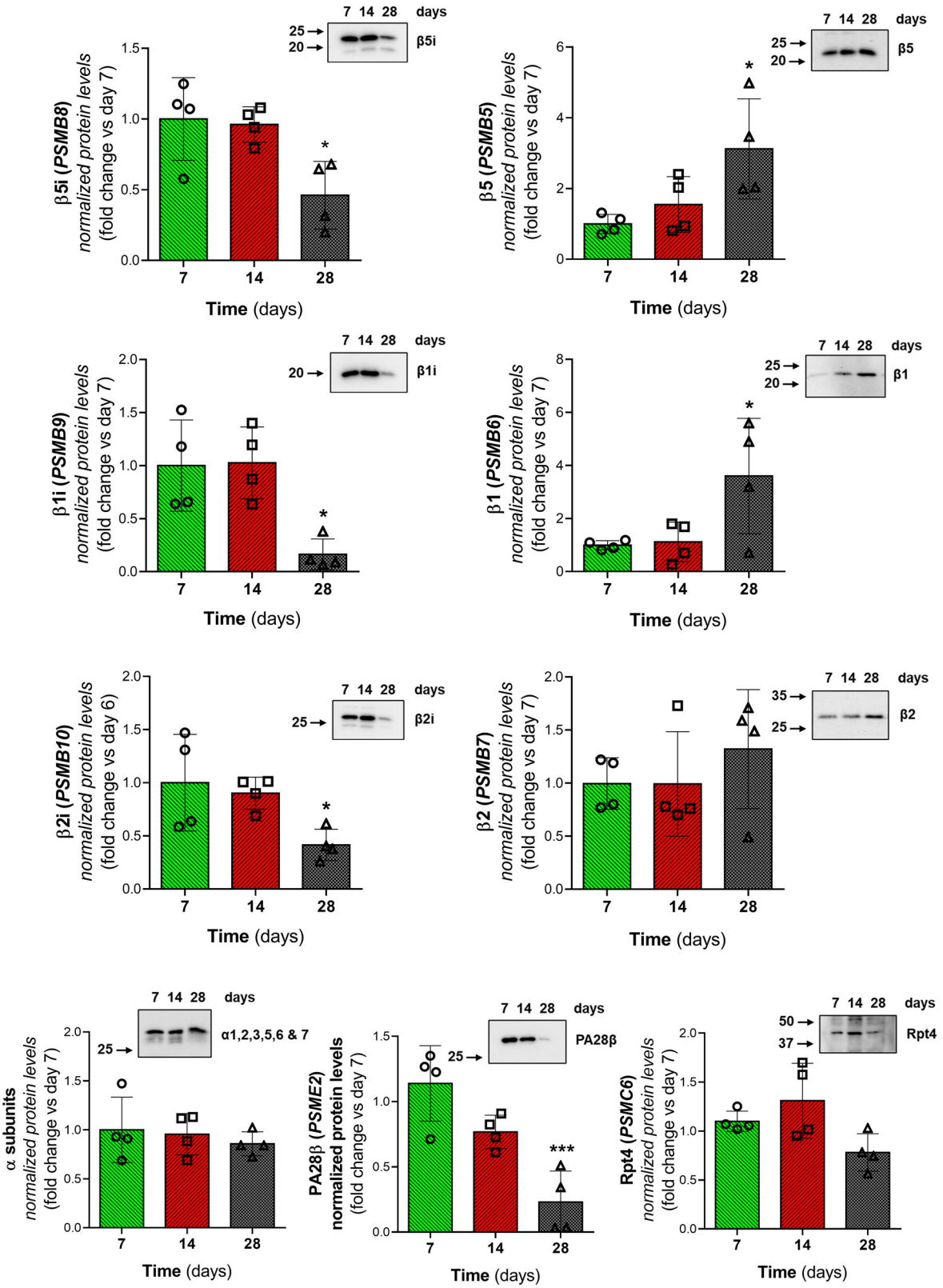

Fig. 4 | Proteasome subunit expression levels. Representative western immunoblot analysis of proteasome (panα, β1, β2, and β5), immunoproteasome (β1i, β2i, and β5i) and regulatory particle (Rpt4 of the 19S RP and PA28β of the PA28αβ RP) subunit expression levels. Two micrograms of total protein was separated by SDS-PAGE on a 12% (w/v) acrylamide gel. The total protein content in each lane was detected using No Stain reagent as a loading control. Immunoreactive bands and total protein signals were imaged with a ChemiDoc system and quantified with Image Lab software. The densitometric values of the immunoreactive bands were normalized to the total protein content and are reported in the graphs as the fold change vs day 7. Data are the mean ± S.D. $^{*}p < 0.05$ and $^{***}p < 0.005$.

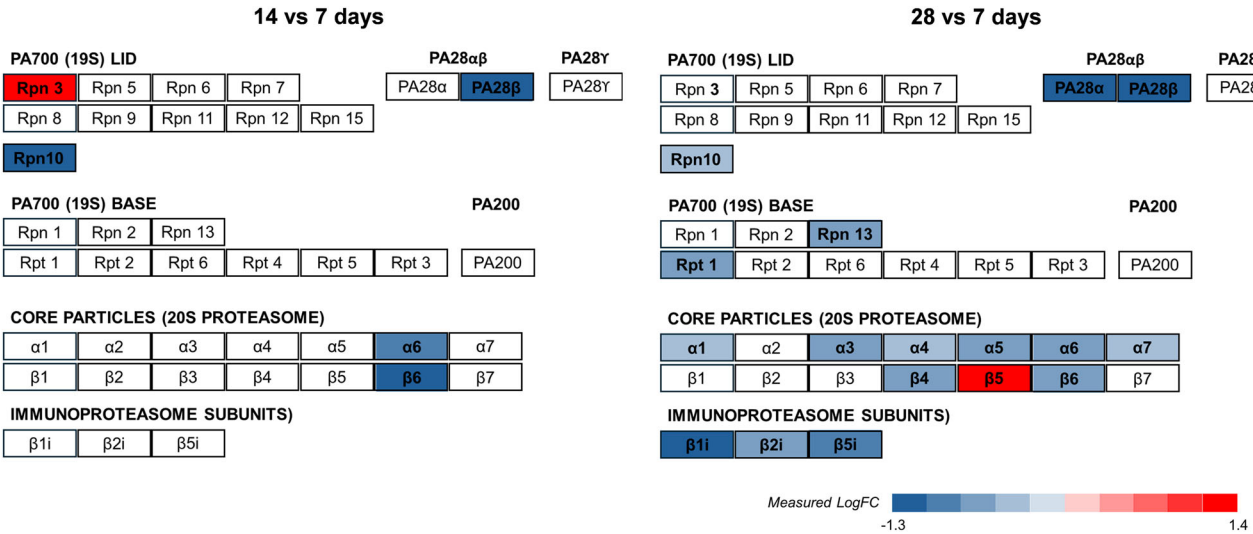

Fig. 5 | Proteomic analysis of differentially expressed proteasome, immunoproteasome and regulatory particle subunits. Differentially expressed proteins within the proteasome pathway (KEGG: hsa03050) were identified via the KEGG ID. Blue indicates downregulation, whereas red indicates upregulation. The intensity of the color varies according to the magnitude of the fold change (FC).

remodeling of the proteasome was irreversible and did not depend on the activation state of the cells. Interestingly, stimulation with IFN-γ promoted the clearance of aggresomes in mature macrophages, probably through autophagy rather than immunoproteasome induction. Indeed, the immunosubunit content and assembly into 20S/PA28αβ complexes did not dramatically increase after stimulation. In contrast, the same structures accumulated in senescent cells, in which not only the immunoproteasome but also the autophagy/lysosomal system were impaired (Fig. 7c).

Loss of PA28αβ capping and the preferential use of 19S-capped proteasomes are hallmarks of immunosenescence in vivo

To determine the relevance of our in vitro results in a model of immunosenescence, we analyzed 20S activity and its assembly with regulatory particles in the lymph nodes of old (18–19-month-old) and young (3–6-month-old) mice (Fig. 8). We chose to study the lymph nodes on the basis of our previous experience and because alterations in the cellularity and functionality of different cell types occur with advancing age[53,54]. Two different mouse strains were investigated: C57BL/6 and BTBR (Fig. 8a, b). C57BL/6 is a widely used strain for aging studies[55]. BTBR mice exhibit abnormal immune functions, increased levels of oxidative stress, and a proinflammatory immune state[56]; therefore, we believe that this model might better recapitulate what we observed in our experimental model of senescent activated macrophages.

Young and old C57BL/6 mice presented similar contents of proteasome complexes, which differed in terms of subunit composition and RP capping (Fig. 8a). In general, lower β5i and greater β5 incorporation were observed in old mice than in young mice. Moreover, old mice presented a lower content of PA28αβ-capped proteasomes with a tendency to assemble 19S-capped holoenzymes.

Consistently, most of the β5i and chymotrypsin-like activities determined by gel assays were associated with the 26S and 30S complexes. Overall, this evidence confirmed the conclusions we drew from the in vitro model. In the case of BTBR, aged mice had more assembled β5i subunits and a lower amount of β5 than young mice did (Fig. 8b). However, they still lost the ability to form PA28αβ-capped complexes with aging; most of the β5i- and chymotrypsin-like activities were indeed catalyzed by 19S-capped complexes, as observed in C57BL/6 mice. Therefore, regardless of the activation state, immune cell senescence seems to involve the inability to form proteasomal complexes with PA28αβ caps and therefore to preferentially use 19S-capped proteasomes.

Discussion

Senescence is defined as irreversible growth arrest in which cells are reprogrammed to survive stress conditions. Growth arrest is also a major characteristic of activated macrophages, some of which survive after an inflammatory response or tissue injury to become tissue-resident macrophages that develop an M2-like phenotype with many features of senescent cells[7,9]. The question of whether mature macrophages represent only a phenotypic state or whether they indeed become senescent upon tissue damage or inflammation is a matter of debate. We established an in vitro model of monocyte-derived senescing macrophages in which, after 7 days of culture, adherent MOs differentiated into activated Mφs. If macrophages were cultured for up to three weeks, they deactivated over time and developed a senescence-like phenotype characterized by cell flattening and enlargement, $p21^{Waf1/Cip1}$ and $p16^{INK4a}$ coexpression, SAβ-gal staining, and lipofuscin accumulation. Owing to the similarity between macrophages and senescent cells, these markers have been debated because they are expressed during monocyte-to-macrophage differentiation and in activated macrophages to sustain their effector function[9]. Under our experimental conditions, these markers appeared in a time window where the cells were already differentiated, as demonstrated by receptor marker expression, and were largely deactivated, as shown by decreased cytokine secretion. Therefore, we considered them bona fide signatures of macrophage senescence.

Activated macrophages displayed many features of proteostasis disturbance, including protein carbonylation, ubiquitination and aggresome formation, which declined with time. It has been demonstrated that the prolonged disturbance of the proteostasis system induces cellular senescence. However, the mechanisms by which proteolytic systems rearrange to maintain protein homeostasis in senescent cells, particularly in immune cells, remain poorly characterized[47]. This aspect is particularly important in nondividing cells, which tend to accumulate damaged material over time.

In this study, we provide evidence that activated mature macrophages predominantly contain PA28αβ-capped immunoproteasome complexes, which are lost during senescence and replaced by 19S-capped proteasomes to maintain proteostasis. The induction of PA28αβ has been observed in dendritic cell maturation by cytokines, bacteria and CD40L as well as in embryonic stem cells (ESs) differentiation[57,58]. These findings raise the possibility that these complexes contribute to macrophage differentiation and activation as well. The role of the PA28αβ/20S complex in the immune system is uncertain, its biology and mechanisms of action are indeed largely unknown and debated. PA28αβ, also known as the 11S complex, is a

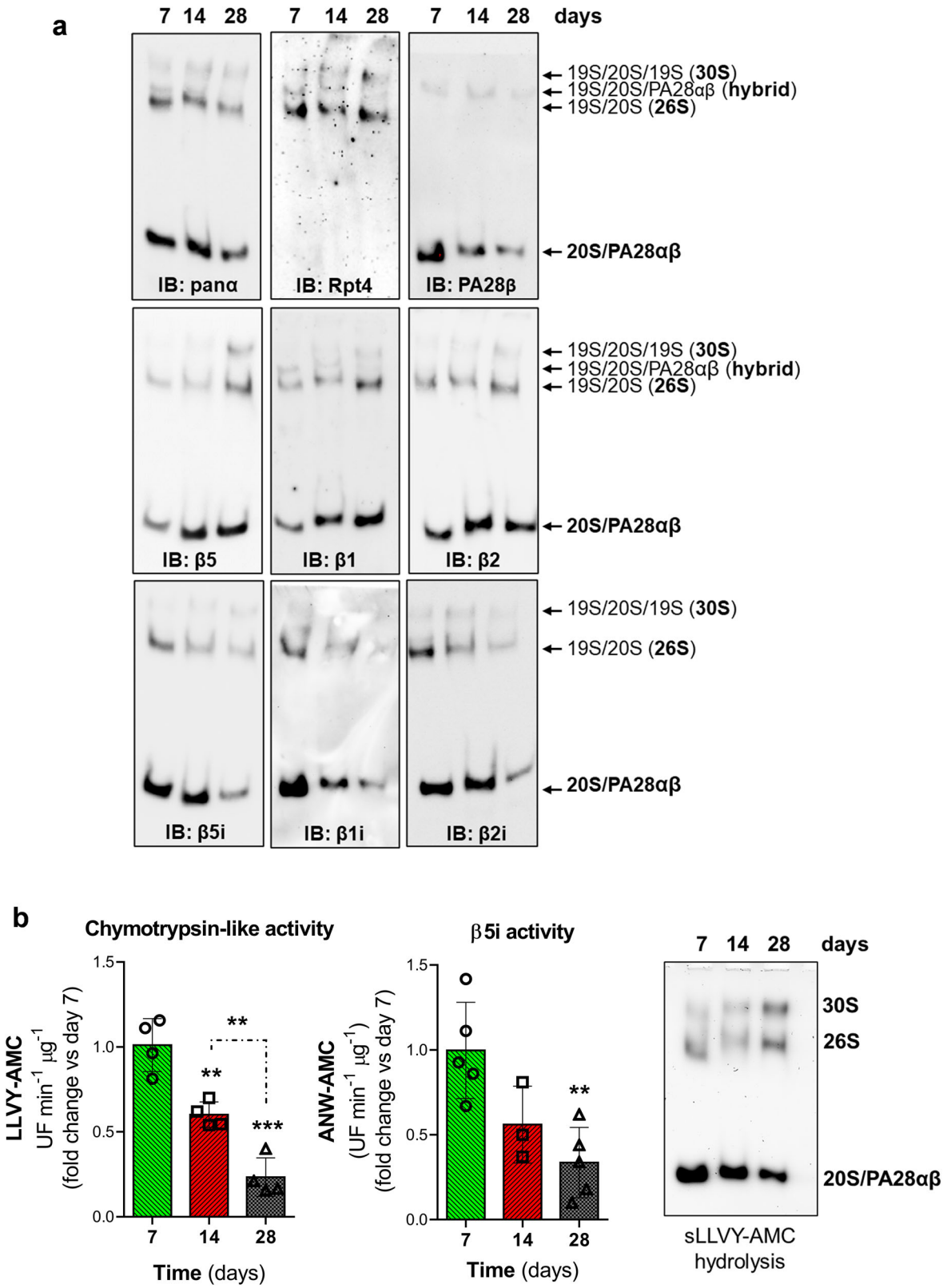

Fig. 6 | Native PAGE of proteasome complexes. a Representative images of native PAGE analysis of proteasome complexes. Native extracts (5 µg for α subunits and 15 µg for β1, β1i, β2, β2i, β5, β5i, Rpt4, and PA28β subunits) were separated on a 4% (w/v) acrylamide gel run under native conditions in the presence of ATP and subjected to western immunoblotting using specific antibodies against the different subunits. Immunoreactive bands were imaged with a ChemiDoc system. IB: immune blot. **b** Proteasome activities were assayed in cell-free extracts obtained under native conditions using the fluorogenic peptide sLLVY-AMC for chymotrypsin-like activity and ANW-AMC for the β5i-associated activity of the immunoproteasome. The activity values are expressed as UF/min/µg protein and are reported in the graphs as the fold change vs day 7. (UF, Units of Fluorescence). Data are the mean ± S.D. $^{**}p < 0.01$; $^{***}p < 0.005$. The image in the right panel represents the "in-gel peptidase activity" using the fluorogenic substrate sLLVY-AMC. After complex separation by native PAGE, the gels were incubated with the substrate, and fluorescent signals were detected in a ChemiDoc system under UV light.

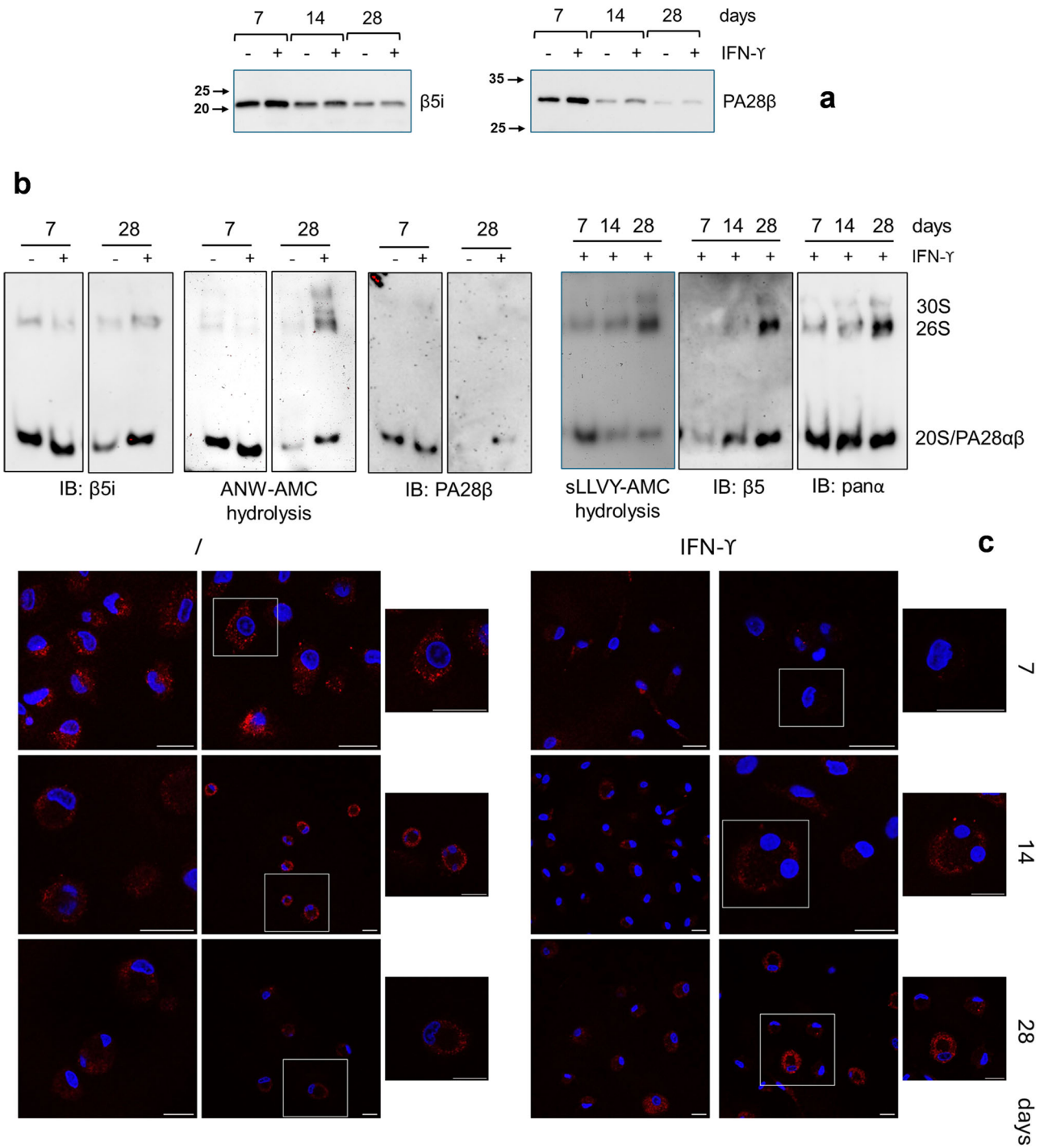

Fig. 7 | Long-term culture of macrophages stimulated with IFN-γ. a Cells were stimulated with IFN-γ and harvested after 24 h. Two micrograms of each macrophage extract was separated via SDS-PAGE on a 12% (w/v) acrylamide gel and subjected to Western immunoblotting with antibodies specific for the β5i subunit of the immunoproteasome and the PA28β subunit of the PA28αβ RP. **b** Native extracts collected after 24 h of IFN-γ stimulation were separated on a 4% (w/v) acrylamide gel under native conditions in the presence of ATP and subjected to western immunoblotting with specific antibodies against the immunoproteasome β5i subunit, PA28β, constitutive β5 subunit and α subunits. sLLVY-AMC and ANW-AMC hydrolysis represent "in-gel peptidase activity", as determined using fluorogenic substrates for chymotrypsin-like and β5i-associated activities, respectively. After native PAGE, the gels were incubated with the specific substrate as indicated, and the activity was detected in a ChemiDoc system under UV light. **c** Aggresome (red) formation under basal and IFN-γ-stimulated conditions was detected with a ProteoStat® Aggresome Detection Kit at 7, 14 and 28 days of culture. DRAQ5 was used to visualize the nuclei (blue). Images were acquired with a confocal Leica microscope (×63 oil objective) using a standard rhodamine filter set. Scale bars 20 μm. IB: immune blot.

proteasome regulator that increases core particle activity in an ATP-independent manner. It has been implicated mainly in MHC I class antigen processing, where it is hypothesized that the PA28αβ/20S/19S complex acts as the proteolytic machinery that generates antigenic peptides, whereas the PA28αβ/20S complex serves to shape them, providing unique repertoires[59]. Recent studies in PA28αβ-knockout mice have demonstrated that PA28αβ is essential for T cell selection in the thymus but not required for mounting an effective immune response against viral infections, thereby casting doubt once more on its involvement in MHC I processing[60]. Moreover, both PA28αβ and the immunoproteasome are induced by oxidative stress; thus, it

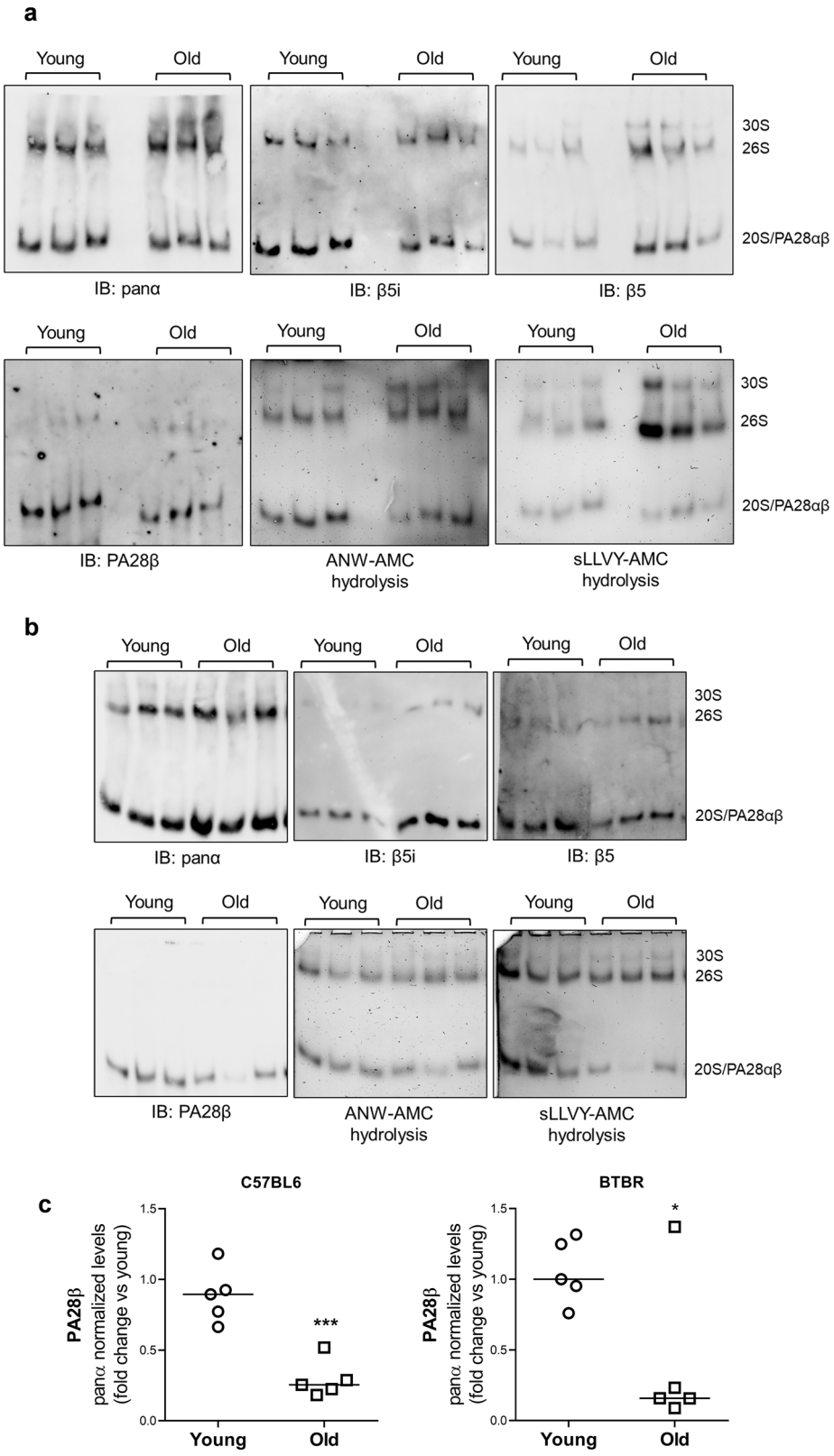

Fig. 8 | Native PAGE analysis of proteasome complexes in the lymph nodes of old and young mice. Representative images of native PAGE analysis of proteasome complexes in the lymph nodes of young and old C57BL/6 (**a**) and BTBR (**b**) mice. Lymph node homogenates (20 μg) were separated on a 4% (w/v) polyacrylamide gel run under native conditions in the presence of ATP and subjected to western immunoblotting using specific antibodies against the immunoproteasome β5i, PA28β, constitutive β5 and α subunits. sLLVY-AMC and ANW-AMC hydrolysis represents "in-gel peptidase activity", as determined using fluorogenic substrates for chymotrypsin-like activity and β5i-associated activity, respectively. After native electrophoresis, the gels were incubated in a solution containing the indicated specific substrates, and the activities were detected in a ChemiDoc system under UV light. **c** The graphs show the quantification of 20S/PA28αβ complexes normalized to the 20S content as determined by the ratio between the PA28β and panα antibody signals. The values obtained from old mice ($n = 5$) are expressed as the fold change vs. values for young mice ($n = 5$). The data sets are depicted as scatter plots where the bar corresponds to the median value. No data points were excluded. $^{*}p < 0.05$; $^{***}p < 0.005$.

has been suggested that these particles may participate in the removal of oxidatively damaged proteins[61]. Unfortunately, the role of the immunoproteasome in maintaining protein homeostasis under inflammatory conditions remains controversial[18].

Macrophage differentiation and activation coincided with the highest accumulation of carbonylated and poly-ubiquitinated proteins, as well as with the formation of aggresomes, suggesting that the PA28αβ/20S complex may be inefficient in removing damaged proteins. However, these proteotoxic stress markers clearly declined during the deactivation phase and the onset of the senescent process, when downregulation of PA28αβ and immunosubunit expression coincided with the loss of the PA28αβ/20S complex and the assembly of 19S-capped proteasomes. In particular, cells

tend to upregulate the expression of and replace immunosubunits with constitutive ones and to cap the core particle with the 19S regulator, a condition that allows the cells to at least partly restore proteostasis. A similar compensatory mechanism involving the upregulation of β5 proteasome subunit expression has been shown to occur upon immunoproteasome inhibition with ONX0914 in activated T cells, alleviating proteostasis stress and preventing apoptotic death[62]. In the case of macrophages, this replacement was irreversible since cells were unable to restore immunosubunit expression after IFN-γ stimulation. The loss of immunosubunit induction by IFN-γ stimulation was also observed in senescent fibroblasts[63]. In aged hippocampal and neuroinflammation models, an interchange between constitutive and immunoproteasome complexes has been associated with decreased proteolytic capacity, which is compensated by autophagy activation[64]. In line with these findings, activated macrophages contained a high number of aggresomes that were rapidly cleared after IFN-γ stimulation. Under these conditions, the inhibitory effect of IL-10 is reversed, and the autophagy pathway is activated[65]. Conversely, IFN-γ stimulation caused aggresome formation in senescent macrophages. Therefore, the formation of 19S-capped complexes is sufficient to maintain protein homeostasis under basal conditions, but not after IFN-γ stimulation because of the acquisition of the senescent-like phenotype, which naturally implies an overall decline in proteolytic systems and a diminished ability to respond to stress[46].

Mechanistically, the shift toward the formation of 19S-capped complexes after downregulation of PA28αβ expression in macrophages can be explained by the fact that PA28αβ and the 19S regulator compete for binding to the 20S catalytic particle; thus, a reduction in PA28αβ levels may result in elevated levels of 19S-capped proteasomes[58]. In cancer cells the preferential use of 19S-capped complexes was associated with the undifferentiated phenotype[66]. Similarly, more 19S-capped proteasomes were found in pluripotent stem cells than in derived neural progenitor cells and neurons[67]. From this perspective, the forced formation of 19S-capped proteasomes together with the interchange between immune and constitutive subunits could drive macrophages toward irreversible dedifferentiation. This possibility is consistent with the idea that senescence is a developmental state resembling dedifferentiation and with the evidence that changes in proteasome dynamics occur in cells undergoing identity changes during differentiation and dedifferentiation[68]. Senescent macrophages exhibited functional changes, including metabolic rewiring, diminished phagocytic activity, and downregulation of splicing and translation factors, reflecting a general loss of specific functions as reported in the literature[16].

The senescence-associated dysfunction of macrophages and other immune cells is an important element of immune deterioration that occurs during aging. This leads to increased susceptibility to infection, autoimmunity, and cancer in elderly individuals. Age-related immune dysfunction is known as immunosenescence, which includes alterations in the composition, quantity and function of immune organs, immune cells and cytokines[69]. Lymph nodes (LNs) are secondary lymphoid organs that coordinate innate and long-term adaptive immune responses that undergo deep structural and functional changes during aging. LNs house various immune cells, including T cells, B cells and antigen-presenting cells such as dendritic cells and macrophages, whose function, development and proliferation capacity are strongly affected during aging[70]. Analysis of proteasome complexes in the lymph nodes of aged mice compared with those of young mice revealed the downregulation of PA28αβ expression and a switch toward the use of 19S capped particles as observed in macrophages. Decreased levels of PA28αβ-capped proteasomes may contribute to explain why immune-specific lymph node functions are impaired in aged mice.

In conclusion, the data presented in this work not only demonstrate that immunoproteasome levels and activity decrease in senescent macrophages, as has been shown for the proteasome in nonimmune cells, but also that this event is accompanied by the remodeling of proteasome complexes with the incorporation of constitutive subunits and capping with the 19S instead of the PA28αβ regulator to maintain proteostasis.

In addition, the results confirmed by in vivo experiments point to the loss of PA28αβ as a hallmark of immunosenescence and a possible target of future therapeutic intervention to improve immune responses in elderly individuals. Although our observations are limited to in vitro activated macrophages devoid of niche support[8] and mouse lymph nodes, the results represent a significant breakthrough in the understanding of the molecular mechanisms underlying immunosenescence, providing a new perspective that deserves further investigation. In the absence of comprehensive knowledge on the PA28αβ regulator, elucidating its role in the development and function of immune cells is essential[71]. Moreover, other lymphoid organs and immune cells and types need to be analyzed to understand the impact of immunoproteasome changes on the deterioration of the immune system during aging. Analyses of single-cell lymph node populations will further shed light on this aspect, considering that different cell types experience different types of dysfunctions. Finally, as women usually show a slower decline in immune function with advancing age than men do, and only male mice were analyzed in this study, it would be interesting to extend these observations to older females as well[72].

Materials and methods

PBMC isolation from leukopacks, monocyte separation and differentiation into macrophages

PBMCs were isolated from leukopacks derived from pathogen-negative human blood processed with the Automated Blood Processing System Reveos (Terumo) to separate platelets (IPU for clinical use) from white cells (leukopacks). Leukopacks were prepared and kindly provided by the Blood Transfusion Center of "Azienda Ospedaliero-Universitaria - Ospedali Riuniti Ancona", Torrette (AN), Italy and "Ospedale S. Maria della Misericordia", Urbino (PU), Italy. Leukopacks were derived from the blood of adult volunteers (aged between 20 and 60) who signed an informed consent prior to donation. Specific ethical approval from the local ethics committee was deemed not applicable for the following reasons: (1) the transfer of the material took place under an agreement between the Azienda Sanitaria Territoriale di Pesaro e Urbino (Italy) and the University of Urbino Carlo Bo, Department of Biomolecular Sciences (protocol no. 1511), which regulates and authorizes the transfer of blood components for research purposes, including monocyte isolation; (2) this study did not involve any interventions or the collection of personal or sensitive data. The blood-derived cells were obtained anonymously from a certified transfusion center, and donor identities were not accessible. All ethical regulations relevant to research involving human participants were followed.

PBMCs were isolated from leukopacks by density gradient centrifugation on a Lymphoprep (Axis Shield, specific density of 1.077) using SepMate-50 tubes following manufacturer's instructions (Stem Cell Technologies, #85450).

PBMCs were resuspended in RPMI 1640 medium (#ECM9106L) supplemented with 10% (v/v) heat-inactivated fetal bovine serum (#ECS5000L), 2 mM glutamine, 100 μg/ml streptomycin, and 100 U/ml penicillin (Euroclone). A total of 14×10^6 cells were seeded in 35 mm diameter Petri dishes treated for increased cell attachment (Avantor, #734-2814). Monocytes were separated from lymphocytes by plastic adhesion after overnight incubation at 37 °C in an atmosphere of 5% CO_2. The next day, nonadherent cells were removed by aspiration, and adherent monocytes were cultured for 7 days in RPMI medium to obtain mature macrophages (herein referred to as monocyte-derived human macrophages or MDMs). The culture medium was changed 3 times a week, and cells were collected 24 h after the last medium change at 7, 14 and 28 days of culture for subsequent analyses. Where indicated, MDMs were stimulated with 100 U/ml recombinant human interferon-γ (Gibco, Thermo Fisher Scientific, #PHC4031) for 24 h.

Animal model

C57BL/6 (B6) and BTBR male mice were reared in the animal shelter of the Department of Biomolecular Sciences at the University of Urbino Carlo Bo. The animals were housed in classical cages, with 3 to 5 mice per cage, with a 12 h light–dark cycle under controlled conditions: temperature (22 ± 1 °C),

humidity (60%) and air exchange (every 12 h). The mice were fed a Teklad Global 18% Protein Rodent Diet (Teklad, Harlan Laboratories Inc., Madison, WI, USA) and provided water ad libitum. The number of mice was established as the minimum number to obtain statistically significant differences. No including and excluding criteria were set. The study did not have humane endpoints. All experiments were conducted in accordance with European legislation (2010/63/EU) and Italian national legislation (DL26/2014) regulating the use of animals for research and the guidelines of Istituto Superiore di Sanità on the use and care of laboratory animals. The study received ethical approval from the OPBA (Organismo Preposto al Benessere Animale, University of Urbino Carlo Bo) and Ministero della Salute - Italy (BTBR mouse authorization no. 486/2017-PR) (C57BL/6 mouse authorization no. 655/2022-PR). We have complied with all relevant ethical regulations for animal use. BTBR mice were wild-type animals belonging to a colony of BTBR PAHENU2 (-/-) mice bred as a model of phenylketonuria; 3-month-old (young group) and 17.8 ± 1.3-month-old (old group) male mice were used for this study. C57BL/6 (B6) male mice were purchased from Charles River Laboratories and sacrificed at 6 months (young group) and 18 months (old group) of age. Lymph nodes from 5 young and 5 old mice per strain were analyzed. Inguinal, axillary, and submandibular lymph nodes from each mouse were excised, immediately frozen in liquid nitrogen and stored at -80 °C.

Cell extracts

Monocyte-derived human macrophages were washed twice with cold PBS and lysed directly in the well by adding a denaturing lysis mixture containing 50 mM Tris-HCl (pH 7.8), 0.25 M sucrose, 2% (w/v) sodium dodecyl sulfate (SDS), and 10 mM N-ethylmaleimide (NEM), supplemented before use with protease inhibitor cocktail (Complete, Roche), 5 mM MG132 and phosphatase inhibitors (1 mM NaF and 1 mM Na_3VO_4). The samples were collected in Eppendorf tubes with the aid of a scraper and warmed at 100 °C for 2 min. The lysates were sonicated at 50 watts for 40 s and centrifuged at 14,000 × *g* to remove cell debris. The supernatant was transferred to a new tube, and the protein concentration was determined by the Lowry's assay using bovine serum albumin (BSA) as a standard.

SDS–PAGE and Western immunoblotting

Proteins were separated by SDS gel electrophoresis (SDS-PAGE) and transferred to a polyvinylidene difluoride (PVDF) membrane with a pore size of 0.2 µm. After transfer, total proteins were visualized on the membrane with the No-Stain™ Protein Labeling Reagent (Invitrogen). The membranes were blocked and then incubated overnight (o/n) at 4 °C with the following primary antibodies (1:1000 dilution): anti-α1,2,3,5,6,7 (#PW8195, pan α) from Enzo Life Sciences; anti-*PSMB6*/β1 (#A4053), anti-*PSMB7*/β2 (#14771), anti-*PSMB10*/β2i (#A5452), anti-19S *PSMC6*/Rpt4 (#A5377), anti-*PSME2*/PA28β (#A5562), anti-$p16^{INK4a}$ (#A11651) from ABclonal; anti-*PSMB8*/β5i (#13635), anti-$p21^{Waf1/Cip1}$ (#2355), anti-LC3B (#2775), anti-PCNA (PC10) (#2586) from Cell Signaling Technology; anti-*PSMB9*/β1i (C-term) (#AP21207b) and anti-*PSMB5*/β5 (#ALS17241) from Abcepta; anti-SQSTM-1/p62 (A302-856A-M) from Bethyl; and anti-Ubiquitin kindly provided by Prof. A.L. Haas, New Orleans School of Medicine (New Orleans, LA, USA). The membranes were then incubated with horseradish peroxidase (HRP)-conjugated secondary antibodies. A WesternBright ECL kit (Enhanced Chemiluminescence, Advasta) was used for the detection of immunoreactive bands, which were visualized on a ChemiDoc MP imaging system (Bio-Rad). The quantification of the immunoreactive signal was performed using Image-Lab software version 5.2.1 (Bio-Rad), and the obtained values were normalized to the total protein content as determined by the No-Stain reagent.

Protein carbonyl assay

Monocyte-derived human macrophages were lysed in buffer consisting of 10 mM HEPES/KOH (pH 7.9), 10 mM KCl, 0.2 mM ethylenediaminetetraacetic acid (EDTA), 0.01% (v/v) Nonidet P-40 and 50 mM dithiothreitol (DTT) supplemented with a cocktail of protease inhibitors. Carbonylated proteins were detected with an OxyBlot™ protein oxidation detection kit (Sigma–Aldrich, #S7150) following the manufacturer's instructions. Each sample (5 µgs) was incubated with 1× 2,4-dinitrophenylhydrazine (DNPH) solution or incubated with only the neutralization solution as a negative control. The samples were loaded on a 12% (w/v) acrylamide gel and transferred to a membrane for Western immunoblotting with antibodies provided in the kit.

Lactate Dehydrogenase assay

Lactate dehydrogenase (LDH) activity was determined using a kinetic spectrophotometric assay based on the oxidation of NADH during the conversion of pyruvate to lactate[73]. Because the number of cells in each well depended on monocyte adhesion, which varied from well to well, and the difficulty of detaching macrophages, especially at 28 days of culture, we measured intracellular LDH activity in native cell extracts as a viability assay and LDH release into the culture medium as an indicator of cell death. The activity of LDH was determined in the extracts and in the medium collected 24 h after the last medium change at 7, 14 and 28 days of culture. Intracellular LDH was expressed as U/µg of protein, and the total amount of LDH released was normalized to the total protein content of the cell lysate derived from the same well to consider variability in cell number between wells.

Native protein extraction from monocyte-derived human macrophages and mice lymph nodes

MDMs/lymph node samples were homogenized using a Teflon pestle in native lysis buffer consisting of 10 mM Tris–HCl (pH 7.5), 5 mM $MgCl_2$, 10 mM NaCl, 10% (v/v) glycerol supplemented with 1 mM DTT, 2 mM ATP, and a protease inhibitor cocktail. The extracts were subsequently centrifuged at 20,000 × *g* for 10 min at 4 °C. The supernatants were transferred to a new tube, and the protein concentration was determined by the Bradford assay (Bio-Rad Laboratories) using BSA as a standard. The lysates were stored at −80 °C in aliquots until analysis.

Native PAGE and gel proteasome assay

Analyses of proteasome complexes via native PAGE were conducted in accordance with the protocol described by Yazgili et al.[74] and Roelofs et al.[75]. Briefly, native protein extracts were diluted in 5x loading buffer consisting of 250 mM Tris-HCl (pH 7.5), 50% (v/v) glycerol and 0.05% (w/v) bromophenol. The proteins were loaded onto 4% (w/v) polyacrylamide gels in Tris/borate (90 mM Tris, 90 mM borate, 5 mM $MgCl_2$, 1 mM EDTA and 0.5 mM ATP) and run at 150 V for 2.5 h at 4 °C. At the end of the run, proteasome complex activity was assayed in the gel using the following synthetic fluorogenic substrates (Cayman Chemicals): s-LLVY-AMC (Suc-Leu-Leu-Val-Tyr-7-amido-4-methylcoumarin) for chymotrypsin-like activity; Boc-LRR-AMC (Boc-Leu-Arg-Arg-AMC) for trypsin-like activity; and Ac-ANW-AMC (Ac-Ala-Asn-Trp-AMC) and Ac-PAL-AMC (Ac-Pro-Ala-Leu-AMC) for β5i- and β1i-specific substrates, respectively. The gels were incubated at 37 °C in the dark in a solution containing 50 mM Tris-HCl (pH 7.5), 2.5 mM ATP/$MgCl_2$, 1 mM DTT and the fluorogenic peptides. Fluorescence emission was detected under UV light in a Chemi-Doc MP imaging system. Proteasome complexes were then denatured by immersing the gel in solubilization buffer consisting of 2% (w/v) SDS, 66 mM Na_2CO_3, and 1.5% (v/v) β-mercaptoethanol (β-MSH). Proteins were transferred to PVDF membranes and labeled with antibodies against the α and β subunits of the proteasome as described above.

Proteasome activity in cell-free extracts

Proteasome activity was assessed in native protein extracts obtained as described above using the following synthetic fluorogenic substrates: s-LLVY-AMC for chymotrypsin-like activity and Ac-ANW-AMC for β5i-associated activity. The assay buffer consisted of 50 mM HEPES/KOH pH 7.8, 5 mM KCl, 2.5 mM ATP and 25 mM $MgCl_2$. The reaction was initiated by the addition of a fluorogenic peptide (200 µM s-LLVY-AMC or 100 µM Ac-ANW-AMC). The release of AMC from the peptidyl derivatives after hydrolysis was measured at 37 °C for 30 min in a FluoStar Optima (BMG

Labtech) fluorimeter with excitation/emission wavelengths of 355/460 nm. Proteasome activity was calculated from the slope after linear regression analysis of the values plotted as a function of time ($R^2 > 0.98$).

Sudan B Black staining

Lipofuscin was detected by Sudan B Black (SBB) staining following the protocol described by Moreno-Blas et al.[36]. MDMs were cultured in 35 mm diameter Petri dishes containing a coverslip, fixed with a 4% (v/v) formaldehyde solution and stained with a saturated SBB solution. The staining was observed under an inverted light microscope, and the cells were considered positive for staining if blue/black granules were evident.

Senescence-associated-β-galactosidase activity (SA-β-Gal) staining

Monocyte-derived human macrophages were fixed with 2% (v/v) formaldehyde and 0.2% (v/v) glutaraldehyde in PBS at RT for 5 min, washed twice in the same buffer, and then incubated at 37 °C for 12 h with fresh X-Gal staining solution (1 mg/ml 5-bromo-4-chloro-3-indolyl ß-D-galactopyranoside) (Sigma, #B4252). The X-Gal staining mixture contained 40 mM citric acid/Na phosphate buffer, 5 mM $K_4[Fe(CN)_6]$ 3 H_2O, 5 mM $K_3[Fe(CN)_6]$, 150 mM NaCl, 2 mM $MgCl_2$ and 1 mg/ml X-Gal[76]. After X-Gal incubation, MDMs were washed for ~30 s twice with PBS. MDMs containing X-Gal crystals (blue precipitate) were visualized using a Nikon Eclipse 80i light microscope (Laboratory Imaging, Czech Republic) with a 60x objective at a final magnification of 750×. Images were obtained with a Sony DS-5M camera connected to an ACT-2U image analyzer.

Immunofluorescence analysis by confocal microscopy

Monocyte-derived human macrophages were grown on 35 mm MatTek glass bottom dishes (MatTek Corporation), washed with PBS and fixed for 15 min with 4% (v/v) paraformaldehyde. MDMs were then washed three times with PBS and permeabilized for 15 min with 0.1% (v/v) Triton X-100. Following three washes with PBS, MDMs were blocked in 2% (w/v) BSA for 1 h and then incubated overnight at 4 °C with the following primary antibodies: anti-$p21^{Waf1/Cip1}$ (mouse, sc-6246, Santa Cruz Biotechnology, 1:100 dilution), anti-$p16^{INK4a}$ (rabbit, #A11651, ABclonal, 1:100 dilution); and anti-Ki67 (rabbit, ab15580, Abcam, 1:1000 dilution). After being (3×) washed with PBS, MDMs were incubated with mouse Alexa Fluor®-conjugated (for p21 staining), rabbit PE-conjugated (for p16 staining) and rabbit FITC-conjugated (for Ki67 staining) secondary antibodies for 1 h, followed by (4×) PBS washes. DRAQ5 (Thermo Fisher, #65-0880) staining was used to visualize the nuclei. Fluorescence images were captured using a confocal Leica microscope (×63 oil objective). KATO III cells were obtained from ATCC (American Type Culture Collection) and cultured in RPMI 1640 medium (Sigma Aldrich), supplemented with Fetal Bovine Serum and antibiotics[66]. These cells were used as positive controls for Ki67 staining.

Detection of aggresomes

Aggregated proteins were detected with a ProteoStat® Aggresome Detection Kit (Enzo Life Sciences Inc,. #ENZ-51035) in accordance with the manufacturer's instructions. Briefly, MDMs were washed twice with PBS and then fixed with 4% (v/v) formaldehyde solution. After washing (2×), the cells were permeabilized with permeabilization solution (0.5% Triton-X-100, 3 mM EDTA, pH 8.0 in 1x Assay Buffer) for 30 min on ice, followed by 2 washes with PBS. Then, the cells were stained with ProteoStat® Aggresome Detection Reagent (1:2000) for 30 min at RT. Nuclei were stained with DRAQ5 dye. Aggregate formation was analyzed using a confocal Leica microscope (×63 oil objective) with a standard rhodamine filter set.

Cytofluorimetric analyses

Cytometric experiments were carried out on a FACSCanto II flow cytometer (BD) equipped with an argon laser (Blue, Excitation 488 nm), a helium-neon laser (Red, Excitation 633 nm), and a solid-state diode laser (Violet, Excitation 405 nm). Analyses were performed with FACSDivaTM software (BD) and Kaluza software (Beckman Coulter). Approximately 10,000 cell events were acquired for each sample.

The phenotypic characterization of monocytes and monocyte-derived human macrophages was performed using the following anti-human monoclonal antibodies for flow cytometry: anti-CD11c (D12-APC), anti-CD11b (SHCL-3-APC), anti-CD206 (19.2-BV421), anti-CD80 (2D10.4-AlexaFluor647), anti-CD14 FITC/CD64 PE (MΦP9, MD22) and anti-TLR4 (TF901-BB700) from BD Pharmingen and anti-CD68 (Y1/82 A, Alexa-Fluor647) from Biolegend. MOs and MDMs were harvested by gentle scraping in culture medium, centrifuged at 300 × *g* for 5 min and resuspended in PBS. Suspensions containing from 7×10^4 to 15×10^4 cells were incubated for 20 min at RT with the indicated fluorophore-conjugated antibodies (1:10 dilution) combined in multicolor panels.

For the assessment of phagocytosis, detached cells were incubated in the presence or absence (negative controls) of 100 µg/ml pHrodo Green zymosan nanoparticles (#P35365; Thermo Fisher) for 1 h at 37 °C. As a negative control for phagocytic activity, samples were incubated on ice.

The lysosome compartment was stained with LysoTracker Green or Deep Red (LTG and LTR, Thermo Fisher Scientific, #L7526 and #L12492). The detached cells were incubated with 100 nM LysoTracker for 30 min in the dark at RT.

For flow cytometric analysis of the cell cycle with propidium iodide (PI) DNA staining, cells were fixed with ice-cold ethanol (70%) and stored at 4 °C. The samples were then washed twice with PBS, and each pellet was suspended in PBS containing 0.02 mg/ml PI (Sigma–Aldrich, #81845) and 0.1 mg/ml RNase A (Roche, #10109142001) before analysis.

Proteomic analysis

Monocyte-derived human macrophages were processed with an EasyPep MS Sample Kit (Thermo Scientific Pierce). Briefly, 100 µl of EasyPep lysis buffer were added to each petri dish and, after scraping, MDMs were collected into tubes. Sample processing was carried out according to manufacturer's instructions. After reduction and alkylation, proteins were digested with trypsin/LysC and peptide content was determined with Pierce Quantitative Colorimetric Peptide Assay kit (#23275, Thermo Scientific Pierce). A total of 1.5 µg of each sample was injected into an UltiMate 3000 RSLC nanosystem coupled to an Exploris 240 mass spectrometer (Thermo Fisher Scientific) and resolved by an Easy-Spray Pepmap RSLC 18 (2 µm, 50 cm × 75 µm) at a flow rate of 250 nL/min with a gradient of phase B (80% acetonitrile/0.1% formic acid, solvent A was 0.1% formic acid in water) from 2% to 40% in 200 min. Then, (B) was changed to 99% at 20 min and maintained for 14 min, and the column was re-equilibrated for 15 min. Data were acquired in positive mode in a data-dependent manner (DDA). The MS1 m/z range was set to 350–1500 at 120,000 resolution (at m/z 200), the AGC target was 3e6, and auto injection time was set. MS2 was switched when the ion intensity was above 5e3, with a m/z range in auto mode, a normalized HCD energy of 30%, an AGC target of 7.5e4, and a maximum injection time of 40 ms. The resolution was set to 15,000 at m/z 200. The internal calibrant was employed in run start mode. Analysis was performed with four technical replicates of each biological sample ($n = 4$).

The raw data generated by Xcalibur 4.2 software (Thermo Fisher Scientific) were analyzed by Proteome Discoverer 2.5 (Thermo Fisher Scientific) using the SEQUEST algorithm. The carbamidomethylation of cysteines was considered a fixed modification, whereas variable serine, threonine or tyrosine phosphorylation was considered. Additionally, the variables oxidation (M) and deamidation (N, Q) were included. The false discovery rate was evaluated by a target-decoy strategy in a concatenated q-value manner. The FDR (strict) was set as 0.01, and the FDR (relaxed) was set as 0.05. Differentially expressed master proteins (log2-fold change of 0.3 and $p < 0.05$) were selected and individually evaluated. Fold changes adjusted *p* values and accession numbers were used to perform pathway analysis using the Advaita's proprietary impact analysis method using iPathwayGuide software (Advaita Corporation Ann Arbor, MI).

RNA preparation and quantitative real-time PCR (qPCR)

Total RNA was extracted using an RNeasy Plus Mini Kit (Qiagen Inc., #74134) in accordance with the manufacturer's instructions. The RNA concentration was measured using a Nanodrop ND-1000 system (NanoDrop Technologies). The RNA (500 ng) was reverse transcribed using PrimeScriptTM RT Master Mix (Perfect Real Time; Takara Bio Europe SAS, #RR036A). cDNA was amplified with each primer pair using a Hot-Rescue Real Time PCR Kit (Diatheva s.r.l., #MBK0011), essentially in accordance with the manufacturer's instructions, and visualized with SYBR Green using an ABI PRISM 7500 Sequence detection system (Applied Biosystems). Thermal cycling was performed as follows: 10 min at 95 °C and 40 cycles of denaturation at 95 °C for 15 s, annealing at 60 °C for 15 s, and extension at 72 °C for 30 s. At the end of the PCR cycles, a melting curve was generated to verify the specificity of the PCR products. All the measurements were performed by testing $n = 3$ technical replicates per sample.

The target gene values were normalized to those of three commonly used housekeeping genes: β2-microglobulin (*β2M*), glyceraldehyde-3-phosphate dehydrogenase (*GAPDH*), and ribosomal RNA 18S (*rRNA 18S*). Expression data were derived via the $2^{-\Delta\Delta Ct}$ method[77]. The final expression value for each target gene was calculated as the geometric mean ± SD of the fold changes versus the 7-day time point obtained with the three different housekeeping genes.

The primers used were as follows: *β2M* (beta 2-microglobulin) *Fwd*: GCCTGCCGTGTGAACCAT, *Rev*: CATCTTCAAACCTCCATGATGCT; *GAPDH* (Glyceraldehyde-3-Phosphate Dehydrogenase) *Fwd*: TGCACCACCAACTGCTTAG, *Rev*: GATGCAGGGATGATGTTC; *18S rRNA* (Ribosomal RNA 18S) *Fwd*: GTAACCCGTTGAACCCCATT, *Rev*: CCATCCAATCGGTAGTAGCG; *PSMB6* (β1) *Fwd*: CAGAACAACCACTGGGTCCT, *Rev*: TGGTAGGTGACAGCATCAGC; *PSMB7* (β2) *Fwd*: GCAACTGAAGGGATGGTTGT, *Rev*: GCTGGGTTGTCATGTCTGTG; *PSMB5* (β5) *Fwd*: ACGTGGACAGTGAAGGGAAC, *Rev*: CTGCTCCACTTCCAGGTCAT; *PSMB9* (β1i) *Fwd*: CAACGTGAAGGAGGTCAGGT, *Rev*: TGCTGCATCCACATAACCAT; *PSMB10* (β2i) *Fwd*: ATACGCGAGCCACTAACGAT, *Rev*: CAGCCCCACAGCAGTAGATT; *PSMB8* (β5i) *Fwd*: GACAGTGGCTATCGGCCTAA, *Rev*: TCACCCAACCATCTTCCTTC.

Secreted cytokine detection

MDM culture medium was collected 48 h after the last medium change, centrifuged and stored at −80 °C. Cytokine levels were measured using a human 9-plex kit (Bio-Rad, #12010316) that included IFN-γ, IL-1β, IL-6, IL-8, IL-10, IL-12p70, IL-12p40, IL-18, and TNF-α, and plate reading was carried out using a Bio-Plex 200 Array Reader® (Bio-Rad) that utilized X-map Luminex® technology. The data were analyzed with the manufacturer's software (Bio-Plex manager software, v.6.1), and the cytokine concentration was determined using a standard curve. The values were normalized to the protein concentration of the cell lysate obtained from the same well as determined by the Bradford method.

Statistics and reproducibility

Statistical analysis of the data was performed by one-way ANOVA followed by the Tukey–Kramer test (multiple comparisons) or Dunnet's test (comparison versus day 7) and two-way ANOVA followed by Bonferroni's multiple comparison test (multiple comparisons; two independent factors) using GraphPad Prism version 8.4.2 for Windows. In the graphs, data points refer to cells isolated from different donors, cultured up to 28 days and harvested at the indicated time points. Analyses were performed using cells obtained from at least 3 different donors. The reproducibility of the cell conditions was ensured by verifying consistent results across at least three independent experiments. Unpaired T-test was used for comparing the two animal groups.

Reporting summary

Further information on research design is available in the Nature Portfolio Reporting Summary linked to this article.

Data availability

The authors declare that all the data supporting the findings of this study are available within the article and its Supplementary Information files. Supplementary Fig. file contains supplementary Figs. 1–8 and fully uncropped images of gels and blots (Supplementary Fig. 9). Supplementary Data 1 includes detailed processed data obtained by Proteome Discoverer software. Supplementary Data 2 and 3 are inferred data from 14 vs 7 days and 28 vs 7 days comparison, respectively. Supplementary Data 4 are values for all data points shown in the graphs. The mass spectrometry proteomics data have been deposited to the ProteomeXchange Consortium via the PRIDE partner repository with the dataset identifier PXD066998.

Received: 29 November 2024; Accepted: 21 August 2025;
Published online: 26 September 2025

References

1. Murray, P. J. et al. Macrophage activation and polarization: nomenclature and experimental guidelines. *Immunity* **41**, 14–20 (2014).
2. Sieweke, M. H. & Allen, J. E. Beyond stem cells: self-renewal of differentiated macrophages. *Science* **342**, 1242974 (2013).
3. Vairo, G., Royston, A. K. & Hamilton, J. A. Biochemical events accompanying macrophage activation and the inhibition of colony-stimulating factor-1-induced macrophage proliferation by tumor necrosis factor-alpha, interferon-gamma, and lipopolysaccharide. *J. Cell. Physiol.* **151**, 630–641 (1992).
4. Xaus, J. et al. Interferon gamma induces the expression of p21waf-1 and arrests macrophage cell cycle, preventing induction of apoptosis. *Immunity* **11**, 103–113 (1999).
5. Mlcochova, P., Winstone, H., Zuliani-Alvarez, L. & Gupta, R. K. TLR4-Mediated Pathway Triggers Interferon-independent G0 arrest and antiviral SAMHD1 activity in macrophages. *Cell Rep.* **30**, 3972–3980.e5 (2020).
6. Maiuthed, A. et al. Cytoplasmic p21 mediates 5-fluorouracil resistance by inhibiting pro-apoptotic Chk2. *Cancers* **10**, 373 (2018).
7. Italiani, P. & Boraschi, D. From monocytes to M1/M2 macrophages: phenotypical vs. functional differentiation. *Front. Immunol.* **5**, 514 (2014).
8. Guilliams, M. & Svedberg, F. R. Does tissue imprinting restrict macrophage plasticity?. *Nat. Immunol.* **22**, 118–127 (2021).
9. Behmoaras, J. & Gil, J. Similarities and interplay between senescent cells and macrophages. *J. Cell Biol.* **220**, e202010162 (2021).
10. Zhou, D., Borsa, M. & Simon, A. K. Hallmarks and detection techniques of cellular senescence and cellular ageing in immune cells. *Aging Cell.* **20**, e13316 (2021).
11. Suzuki, K., Susaki, E. A. & Nagaoka, I. Lipopolysaccharides and cellular senescence: involvement in atherosclerosis. *Int. J. Mol. Sci.* **23**, 11148 (2022).
12. Su, L. et al. Potential role of senescent macrophages in radiation-induced pulmonary fibrosis. *Cell Death Dis.* **12**, 527 (2021).
13. Carver, C. M. et al. Senescent and disease-associated microglia are modifiable features of aged brain white matter. *Res. Sq. rs.* **3**, 3467812 (2023).
14. Hartman, T. K., Wengenack, T. M., Poduslo, J. F. & van Deursen, J. M. Mutant mice with small amounts of BubR1 display accelerated age-related gliosis. *Neurobiol. Aging* **28**, 921–927 (2007).
15. Rattanaprukskul, K. et al. Molecular signatures of senescence in periodontitis: clinical insights. *J. Dent. Res.* **103**, 800–808 (2024).
16. Wang, L. et al. Macrophage senescence in health and diseases. *Acta Pharm. Sin. B* **14**, 1508–1524 (2024).
17. Hamazaki, J. & Murata, S. Relationships between protein degradation, cellular senescence, and organismal aging. *J. Biochem.* **175**, 473–480 (2024).
18. Basler, M. & Groettrup, M. On the role of the immunoproteasome in protein homeostasis. *Cells* **10**, 3216 (2021).

19. Kasahara, M. Role of immunoproteasomes and thymoproteasomes in health and disease. *Pathol. Int.* **71**, 371–382 (2021).
20. Emmerich, N. P. et al. The human 26 S and 20 S proteasomes generate overlapping but different sets of peptide fragments from a model protein substrate. *J. Biol. Chem.* **275**, 21140–21148 (2000).
21. Raule, M. et al. PA28αβ reduces size and increases hydrophilicity of 20S immunoproteasome peptide products. *Chem. Biol.* **21**, 470–480 (2014).
22. Ehlinger, A. & Walters, K. J. Structural insights into proteasome activation by the 19S regulatory particle. *Biochemistry* **52**, 3618–3628 (2013).
23. Huber, E. M. & Groll, M. The mammalian proteasome activator PA28 forms an asymmetric $\alpha_4\beta_3$. *Complex. Struct.* **25**, 1473–1480.e3 (2017).
24. Matacchione, G. et al. Senescent macrophages in the human adipose tissue as a source of inflammaging. *GeroScience* **44**, 1941–1960 (2022).
25. Wang, H. et al. BRD4 contributes to LPS-induced macrophage senescence and promotes progression of atherosclerosis-associated lipid uptake. *Aging* **12**, 9240–9259 (2020).
26. Fu, Y. et al. Unveiling the role of ABI3 and hub senescence-related genes in macrophage senescence for atherosclerotic plaque progression. *Inflamm. Res.* **73**, 65–82 (2024).
27. Danish, M. et al. Comparative evaluation of cellular senescence in naturally aged and stress-induced murine macrophages for identifying optimum senescent macrophage study systems. *Mol. Biol. Rep.* **52**, 123 (2025).
28. Moss, C. E. et al. Aging-related defects in macrophage function are driven by MYC and USF1 transcriptional programs. *Cell Rep.* **43**, 114073 (2024).
29. Kelly, A., Grabiec, A. M. & Travis, M. A. Culture of human monocyte-derived macrophages. *Methods Mol. Biol.* **1784**, 1–11 (2018).
30. Gažová, I. et al. The transcriptional network that controls growth arrest and macrophage differentiation in the human myeloid leukemia cell line THP-1. *Front. Cell Dev. Biol.* **8**, 498 (2020).
31. Lomovskaya, Y. V. et al. Macrophage-like THP-1 cells derived from high-density cell culture are resistant to TRAIL-induced cell death via down-regulation of death-receptors DR4 and DR5. *Biomolecules* **12**, 150 (2022).
32. Luque-Martin, R. et al. IFN-γ drives human monocyte differentiation into highly proinflammatory macrophages that resemble a phenotype relevant to psoriasis. *J. Immunol.* **207**, 555–568 (2021).
33. Daigneault, M., Preston, J. A., Marriott, H. M., Whyte, M. K. & Dockrell, D. H. The identification of markers of macrophage differentiation in PMA-stimulated THP-1 cells and monocyte-derived macrophages. *PloS One* **5**, e8668 (2010).
34. Mlcochova, P. et al. A G1-like state allows HIV-1 to bypass SAMHD1 restriction in macrophages. *EMBO J.* **36**, 604–616 (2017).
35. Chen, S. et al. Macrophages in immunoregulation and therapeutics. *Signal Transduct. Target. Ther.* **8**, 207 (2023).
36. Moreno-Blas, D. et al. Cortical neurons develop a senescence-like phenotype promoted by dysfunctional autophagy. *Aging* **11**, 6175–6198 (2019).
37. Holt, D. J. & Grainger, D. W. Senescence and quiescence induced compromised function in cultured macrophages. *Biomaterials* **33**, 7497–7507 (2012).
38. Smith, R. et al. A new model and precious tool to study molecular mechanisms of macrophage aging. *Aging* **16**, 12697–12725 (2024).
39. Herranz, N. & Gil, J. Mechanisms and functions of cellular senescence. *J. Clin. Invest.* **128**, 1238–1246 (2018).
40. Kramer, J. L., Baltathakis, I., Alcantara, O. S. & Boldt, D. H. Differentiation of functional dendritic cells and macrophages from human peripheral blood monocyte precursors is dependent on expression of p21 (WAF1/CIP1) and requires iron. *Br. J. Haematol.* **117**, 727–734 (2002).
41. Kumari, R. & Jat, P. Mechanisms of cellular senescence: cell cycle arrest and senescence associated secretory phenotype. *Front. Cell Dev. Biol.* **9**, 645593 (2021).
42. Asada, M. et al. Apoptosis inhibitory activity of cytoplasmic p21(Cip1/WAF1) in monocytic differentiation. *EMBO J.* **18**, 1223–1234 (1999).
43. Coryell, P. R. et al. Autophagy regulates the localization and degradation of p16INK4a. *Aging Cell* **19** e13171 (2020).
44. Zhang, L. M. et al. Interleukin-18 promotes fibroblast senescence in pulmonary fibrosis through down-regulating Klotho expression. *Biomed. Pharmacother.* **113**, 108756 (2019).
45. Fan, Y. et al. Senescent-like macrophages mediate angiogenesis for endplate sclerosis via IL-10 secretion in male mice. *Nat. Commun.* **15**, 2939 (2024).
46. Sabath, N. et al. Cellular proteostasis decline in human senescence. *Proc. Natl. Acad. Sci. USA* **117**, 31902–31913 (2020).
47. Takenaka, Y., Inoue, I., Nakano, T., Ikeda, M. & Kakinuma, Y. Prolonged disturbance of proteostasis induces cellular senescence via temporal mitochondrial dysfunction and subsequent mitochondrial accumulation in human fibroblasts. *FEBS J.* **289**, 1650–1667 (2022).
48. Zhang, C. et al. Autophagic sequestration of SQSTM1 disrupts the aggresome formation of ubiquitinated proteins during proteasome inhibition. *Cell. Death Dis.* **13**, 615 (2022).
49. Seifert, U. et al. Immunoproteasomes preserve protein homeostasis upon interferon-induced oxidative stress. *Cell* **142**, 613–624 (2010).
50. Zhang, H., Puleston, D. J. & Simon, A. K. Autophagy and immune senescence. *Trends Mol. Med.* **22**, 671–686 (2016).
51. Inholz, K. et al. Proteasome composition in immune cells implies special immune-cell-specific immunoproteasome function. *Eur. J. Immunol.* **54**, e2350613 (2024).
52. Sahoo, M. P., Lavy, T., Cohen, N., Sahu, I. & Kleifeld, O. Activity-guided proteomic profiling of proteasomes uncovers a variety of active (and inactive) proteasome species. *Mol. Cell. Proteom.***23**, 100728 (2024).
53. Crinelli, R. et al. A synthetic thiol molecule releasing N-acetyl-l-cysteine and cysteamine drives early up-regulation of immunoproteasome subunits in the lymph nodes of mice infected with LP-BM5 leukemia retrovirus. *Biochim. Biophys. Acta Mol. Basis Dis.* **1870**, 166918 (2024).
54. Budamagunta, V., Foster, T. C. & Zhou, D. Cellular senescence in lymphoid organs and immunosenescence. *Aging* **13**, 19920–19941 (2021).
55. Mitchell, S. J., Scheibye-Knudsen, M., Longo, D. L. & de Cabo, R. Animal models of aging research: implications for human aging and age-related diseases. *Annu. Rev. Anim. Biosci.* **3**, 283–303 (2015).
56. Mutovina, A. et al. Unique features of the immune response in BTBR mice. *Int. J. Mol. Sci.* **23**, 15577 (2022).
57. Macagno, A. et al. Dendritic cells up-regulate immunoproteasomes and the proteasome regulator PA28 during maturation. *Eur. J. Immunol.* **29**, 4037–4042 (1999).
58. Hernebring, M. et al. Removal of damaged proteins during ES cell fate specification requires the proteasome activator PA28. *Sci. Rep.* **3**, 1381 (2013).
59. Cascio, P., Call, M., Petre, B. M., Walz, T. & Goldberg, A. L. Properties of the hybrid form of the 26S proteasome containing both 19S and PA28 complexes. *EMBO J.* **21**, 2636–2645 (2002).
60. Inholz, K., Bader, U., Mundt, S. & Basler, M. The significant role of PA28αβ in $CD8^+$ T cell-mediated graft rejection contrasts with its negligible impact on the generation of MHC-I ligands. *Int. J. Mol. Sci.* **25**, 5649 (2024).
61. Pickering, A. M. et al. The immunoproteasome, the 20S proteasome and the PA28αβ proteasome regulator are oxidative-stress-adaptive proteolytic complexes. *Biochem. J.* **432**, 585–594 (2010).
62. Schmidt, C., Berger, T., Groettrup, M. & Basler, M. Immunoproteasome inhibition impairs T and B cell activation by

restraining ERK signaling and proteostasis. *Front. Immunol.* **9**, 2386 (2018).
63. Stratford, F. L., Chondrogianni, N., Trougakos, I. P., Gonos, E. S. & Rivett, A. J. Proteasome response to interferon-gamma is altered in senescent human fibroblasts. *FEBS Lett.* **580**, 3989–3994 (2006).
64. Pintado, C., Macías, S., Domínguez-Martín, H., Castaño, A. & Ruano, D. Neuroinflammation alters cellular proteostasis by producing endoplasmic reticulum stress, autophagy activation and disrupting ERAD activation. *Sci. Rep.* **7**, 8100 (2017).
65. Matsuzawa, T., Fujiwara, E. & Washi, Y. Autophagy activation by interferon-γ via the p38 mitogen-activated protein kinase signalling pathway is involved in macrophage bactericidal activity. *Immunology* **141**, 61–69 (2014).
66. Monittola, F. et al. Gastric cancer cell types display distinct proteasome/immunoproteasome patterns associated with migration and resistance to proteasome inhibitors. *J. Cancer Res. Clin. Oncol.* **149**, 10085–10097 (2023).
67. Vilchez, D. et al. Increased proteasome activity in human embryonic stem cells is regulated by PSMD11. *Nature* **489**, 304–308 (2012).
68. Schröter, F. & Adjaye, J. The proteasome complex and the maintenance of pluripotency: sustain the fate by mopping up?. *Stem Cell Res. Ther.* **5**, 24 (2014).
69. Pawelec, G. Age and immunity: what is "immunosenescence"?. *Exp. Gerontol.* **105**, 4–9 (2018).
70. Turner, V. M. & Mabbott, N. A. Structural and functional changes to lymph nodes in ageing mice. *Immunology* **151**, 239–247 (2017).
71. Cascio, P. PA28αβ: the enigmatic magic ring of the proteasome?. *Biomolecules* **4**, 566–584 (2014).
72. Calabrò, A., Accardi, G., Aiello, A., Caruso, C. & Candore, G. Sex and gender affect immune aging. *Front. Aging* **4**, 1272118 (2023).
73. Beutler, E. Lactate deydrogenase (LDH). in *Red Cell Metabolism. A Manual of Biochemical Methods* (ed Beutler, E.) 65−66 (Grune and Stratton, Inc., 1984).
74. Yazgili, A. S. et al. In-gel proteasome assay to determine the activity, amount, and composition of proteasome complexes from mammalian cells or tissues. *STAR Protoc.* **2**, 100526 (2021).
75. Roelofs, J., Suppahia, A., Waite, K. A. & Park, S. Native gel approaches in studying proteasome assembly and chaperones. *Methods Mol. Biol.* **1844**, 237–260 (2018).
76. Debacq-Chainiaux, F., Erusalimsky, J. D., Campisi, J. & Toussaint, O. Protocols to detect senescence-associated beta-galactosidase (SA-betagal) activity, a biomarker of senescent cells in culture and in vivo. *Nat. Protoc.* **4**, 1798–1806 (2009).
77. Livak, K. J. & Schmittgen, T. D. Analysis of relative gene expression data using real-time quantitative PCR and the 2(-Delta Delta C(T)) method. *Methods* **25**, 402–408 (2001).

Acknowledgements

This work has been funded by the University of Urbino (grant DISB_CRINELLI_PROG_SIC_ALIMENTARE to R.C.) and by the European Union - NextGenerationEU, Mission 4, Component 2, under the Italian Ministry of University and Research (MUR) National Innovation Ecosystem grant ECS00000041 - VITALITY - CUP H33C22000430006. We are grateful to Dr. Chiara Rychlicki MD, Blood Transfusion Center of "Azienda Ospedaliero-Universitaria - Ospedali Riuniti Ancona", Torrette (AN), Italy, and Dr. Gianluca Riganello MD, "Ospedale S. Maria della Misericordia", Urbino (PU), Italy, for providing leukopacks. We also thank Claudia Scopa and Francesca Pierigè for their help in animal handling; Dr. Genny Del Zotto PhD, Department of Research and Diagnostics, Istituto G. Gaslini, Genoa, Italy, for providing the anti-CD68 antibody; and Prof. Vincenzo Bronte, Istituto Oncologico Veneto, IRCCS, for advice on macrophage phenotyping.

Author contributions

F.M., S.M., M.Mo, M.G.N., A.R., R.D., F.L., M.B., B.C., M.Me, A.F., and R.C.: investigation, data curation, validation and visualization. D.L.: investigation. R.C. and M.M.: resources and editing. R.C. and A.F.: conceptualization, supervision. The first draft of the manuscript was written by R.C. and F.M., and all the authors commented on previous versions of the manuscript. R.C., F.M., M.Me, B.C., M.Mo, F.L., M.G.N.: manuscript revision. All the authors read and approved the final version.

Competing interests

The authors declare no competing interests.

Additional information

Supplementary information The online version contains supplementary material available at https://doi.org/10.1038/s42003-025-08765-7.

Correspondence and requests for materials should be addressed to Rita Crinelli.

Peer review information *Communications Biology* thanks Roel De Maeyer and the other, anonymous, reviewer(s) for their contribution to the peer review of this work. Primary Handling Editor: David Favero. A peer review file is available.